Yamashita A, Salam KA, Furuta A, Matsuda Y, Fujita O, Tani H, Fujita Y, Fujimoto Y, Ikeda M, Kato N, Sakamoto N, Maekawa S, Enomoto N, Nakakoshi M, Tsubuki M, Sekiguchi Y, Tsuneda S, Akimitsu N, Noda N, Tanaka J, Moriishi K.	Inhibition of hepatitis C virus replication and viral helicase by ethyl acetate extract of the marine feather star Alloeocomatella polycladia.	*Mar Drugs.*	10(4)	744-61.	2012
Kazuhiro Haraguchi	Tuning Efficiency of the 4-*Exo-trig* Cyclization by Electronic Effect: Ring-Closure of 3,3-Difluoro-4-pentenyl Carbon Radicals and Synthesis of *gem*-Difluorocyclobutane Nucleoside	*Chem. Commun.*	48	10993-10997	2012
Kazuhiro Haraguchi	From the chemistry of epoxy-sugar nucleosides to the discovery of anti-HIV agent Festinavir	*Current Pharmaceutical Design*	19	1880-1897	2013
Tanyaradzwa P. Ndongwe, Adeyemi O. Adedeji, Eleftherios Michailidis, Yee Tsuey Ong, Atsuko Hachiya, Bruno Marchand, Emily M. Ryan, Devendra K. Rai, Karen A. Kirby, Angela S. Whatley, Donald H. Burke, Marc Johnson, Shilei Ding, Yi-Min Zheng, Shan-Lu Liu, Ei-Ichi Kodama, Krista A. Delviks-Frankenberry, Vinay K. Pathak, Hiroaki Mitsuya, Michael A. Parniak, Kamalendra Singh, Stefan G. Sarafianos	Biochemical, inhibition, and inhibitor resistance studies of xenotropic murine leukemia virus-related virus reverse transcriptase.	*Nucleic Acids Research*	40	345-359	2012
Xiaoguang Li, Hua Qian, Fusako Miyamoto, Takeshi Naito, Kumi Kawaji, Kazumi Kajiwara, Toshio Hattori, Masao Matsuoka, Kentaro Watanabe, Shinya Oishi, Nobutaka Fujii, Eiichi N. Kodama	A simple, rapid, and sensitive system for the evaluation of anti-viral drugs in rats	*Biochemical and Biophysical Research Communications*	424	257-261	2012

Atsuko Hachiya, Bruno Marchand, Karen A. Kirby, Eleftherios Michailidis, Xiongying Tu, Krzystof Palczewski, Yee Tsuey Ong, Daniel T. Griffin, Matthew M. Schuckmann, Junko Tanuma, Shinichi Oka, Kamalendra Singh, Eiichi N. Kodama and Stefan G. Sarafianos	HIV-1 reverse transcriptase (RT) polymorphism 172K, suppresses the effect of clinically relevant drug resistance mutations to both nucleoside and nonnucleoside RT inhibitors.	*Journal of Biological Chemistry*	287	29988-29999	2012
Michailidis E, Singh K, Ryan EM, Hachiya A, Ong YT, Kirby KA, Marchand B, Kodama EN, Mitsuya H, Parniak MA, Sarafianos SG	Effect of translocation defective reverse transcriptase inhibitors on the activity of n348i, a connection subdomain drug resistant hiv-1 reverse transcriptase mutant.	*Cell Mol Biol*	58	187-195	2012
児玉栄一、宮本総子	新しい抗ウイルス剤開発の考え方	*臨床と微生物*	40	51-55	2013
Sakamoto T, Tanaka Y, Kani S, Sugiyama M, Watanabe T, Iijima S, Murakami S, Matsuura K, Kusakabe A, Shinkai N, Sugauchi F, Mizokami M.	Mechanism of the Dependence of Hepatitis B Virus Genotype G on Co-infection with Other Genotypes for Viral Replication.	*J Viral Hepat.*	20	e27-e36	2013
Rawal RK, Singh US, Chavre SN, Wang J, Sugiyama M, Hung W, Govindarajan R, Korba B, Tanaka Y, Chu CK.	2'-Fluoro-6'-methylene-carbocyclic adenosine phosphoramidate (FMCAP) prodrug: In vitro anti-HBV activity against the lamivudine-entecavir resistant triple mutant and its mechanism of action.	*Bioorg Med Chem Lett.*	23(2)	503-6	2013
Ragheb M, Elkady A, Tanaka Y, Murakami S, Attia FM, Hassan AA, Hassan MF, Shedid MM, Abdel Reheem HB, Khan A, Mizokami M.	Multiple intra-familial transmission patterns of hepatitis B virus genotype D in north-eastern Egypt.	*J Med Virol.*	84(4)	587-95	2012
Nishioka T, Yasutake Y, Nishiya Y, Tamura T.	Structure-guided mutagenesis for the improvement of substrate specificity of Bacillus megaterium glucose 1-dehydrogenase IV	*FEBS J.*	279	3264-3275	2012
Takeuchi J, Maehashi K, Yasutake Y, Muramatsu Y, Miyata K, Watanabe T, Nagashima T	Properties of emu (Dromaius novaehollandiae) albumen proteins	*Food Res. Int.*	49	567-571	2012
Kitahara K, Yasutake Y, Miyazaki K	Mutational robustness of 16S ribosomal RNA, shown by experimental horizontal gene transfer in Escherichia coli	*Proc. Natl. Acad. Sci. USA*	109	19220-19225	2012

Ⅳ．研究成果の刊行物・別刷

Antimicrobial Agents and Chemotherapy

GRL-0519, a Novel Oxatricyclic Ligand-Containing Nonpeptidic HIV-1 Protease Inhibitor (PI), Potently Suppresses Replication of a Wide Spectrum of Multi-PI-Resistant HIV-1 Variants *In Vitro*

Masayuki Amano, Yasushi Tojo, Pedro Miguel Salcedo-Gómez, Joseph Richard Campbell, Debananda Das, Manabu Aoki, Chun-Xiao Xu, Kalapala Venkateswara Rao, Arun K. Ghosh and Hiroaki Mitsuya

Antimicrob. Agents Chemother. **2013, 57(5):2036. DOI: 10.1128/AAC.02189-12.**
Published Ahead of Print 12 February 2013.

AAC
Journals.ASM.org

GRL-0519, a Novel Oxatricyclic Ligand-Containing Nonpeptidic HIV-1 Protease Inhibitor (PI), Potently Suppresses Replication of a Wide Spectrum of Multi-PI-Resistant HIV-1 Variants *In Vitro*

Masayuki Amano,[a] Yasushi Tojo,[a] Pedro Miguel Salcedo-Gómez,[a] Joseph Richard Campbell,[a] Debananda Das,[d] Manabu Aoki,[a,b] Chun-Xiao Xu,[c] Kalapala Venkateswara Rao,[c] Arun K. Ghosh,[c] Hiroaki Mitsuya[a,d]

Departments of Infectious Diseases and Hematology, Kumamoto University School of Medicine, Kumamoto, Japan[a]; Department of Medical Technology, Kumamoto Health Science University, Kumamoto, Japan[b]; Departments of Chemistry and Medicinal Chemistry, Purdue University, West Lafayette, Indiana, USA[c]; Experimental Retrovirology Section, HIV and AIDS Malignancy Branch, National Cancer Institute, National Institutes of Health, Bethesda, Maryland, USA[d]

We report that GRL-0519, a novel nonpeptidic human immunodeficiency virus type 1 (HIV-1) protease inhibitor (PI) containing *tris*-tetrahydrofuranylurethane (*tris*-THF) and a sulfonamide isostere, is highly potent against laboratory HIV-1 strains and primary clinical isolates (50% effective concentration [EC_{50}], 0.0005 to 0.0007 μM) with minimal cytotoxicity (50% cytotoxic concentration [CC_{50}], 44.6 μM). GRL-0519 blocked the infectivity and replication of HIV-1_{NL4-3} variants selected by up to a 5 μM concentration of ritonavir, lopinavir, or atazanavir (EC_{50}, 0.0028 to 0.0033 μM). GRL-0519 was also potent against multi-PI-resistant clinical HIV-1 variants isolated from patients who no longer responded to existing antiviral regimens after long-term antiretroviral therapy, highly darunavir (DRV)-resistant variants, and HIV-2_{ROD}. The development of resistance against GRL-0519 was substantially delayed compared to other PIs, including amprenavir (APV) and DRV. The effects of nonspecific binding of human serum proteins on GRL-0519's antiviral activity were insignificant. Our analysis of the crystal structures of GRL-0519 (3OK9) and DRV (2IEN) with protease suggested that the *tris*-THF moiety, compared to the *bis*-THF moiety present in DRV, has greater water-mediated polar interactions with key active-site residues of protease and that the *tris*-THF moiety and parametoxy group effectively fill the S2 and S2′ binding pockets, respectively, of the protease. The present data demonstrate that GRL-0519 has highly favorable features as a potential therapeutic agent for treating patients infected with wild-type and/or multi-PI-resistant variants and that the *tris*-THF moiety is critical for strong binding of GRL-0519 to the HIV protease substrate binding site and appears to be responsible for its favorable antiretroviral characteristics.

Combination antiretroviral therapy (cART) has had a major impact on the AIDS epidemic in industrially advanced nations. Recent analyses have revealed that mortality rates for human immunodeficiency virus type 1 (HIV-1)-infected persons have become close to those of the general population (1–4). However, eradication of HIV-1 does not appear to be currently possible, in part due to the viral reservoirs remaining in blood and infected tissues. Moreover, we have encountered a number of challenges in bringing the optimal benefits of the currently available therapeutics for AIDS and HIV-1 infection to individuals receiving cART (5–7). They include (i) drug-related toxicities, (ii) inability to fully restore normal immunologic functions once individuals developed AIDS, (iii) development of various cancers as a consequence of survival prolongation, (iv) flaring up of inflammation in individuals receiving cART or immune reconstruction syndrome (IRS), and (v) increased cost of antiviral therapy. Such limitations and flaws of cART are exacerbated by the development of drug-resistant HIV-1 variants (8–12), although the recent first-line cART with boosted protease inhibitor (PI)-based regimens has made the development of HIV-1 resistance less likely over an extended period of time (13).

Successful antiviral drugs, in theory, produce their virus-specific effects by interacting with viral receptors, virus-encoded enzymes, viral structural components, viral genes, or their transcripts without disturbing cellular metabolism or function. However, at present, no antiretroviral drugs or agents are likely to be completely specific for HIV-1 or to be devoid of toxicity or side effects in the therapy of AIDS. This is a critical issue, because patients with AIDS and its related diseases will have to receive antiretroviral therapy for a long time, perhaps for the rest of their lives. Thus, the identification of new classes of antiretroviral drugs that have a unique mechanism(s) of action and produce no or minimal side effects remains an important therapeutic objective.

We have been focusing on the design and synthesis of nonpeptidyl PIs that are potent against HIV-1 variants resistant to the currently approved PIs. One such anti-HIV-1 agent, darunavir (DRV) (Fig. 1), containing a structure-based designed privileged nonpeptidic P2 ligand, 3(*R*),3a(*S*),6a(*R*)-*bis*-tetrahydrofuranylurethane (*bis*-THF) (14–16), has been approved as a first-line therapeutic agent for the treatment of individuals who are infected with HIV-1. In the present work, we examined and characterized the nonpeptidic HIV-1 protease inhibitors GRL-0519 (17) and its stereoisomer, GRL-0529, both of which contain the *tris*-THF moiety and a sulfonamide isostere. We found that GRL-0519 exerts highly potent activity against a wide spectrum of laboratory HIV-1

Received 8 November 2012 Returned for modification 3 December 2012
Accepted 5 February 2013
Published ahead of print 12 February 2013
Address correspondence to Hiroaki Mitsuya, hm21q@nih.gov.
Supplemental material for this article may be found at http://dx.doi.org/10.1128/AAC.02189-12.

doi:10.1128/AAC.02189-12

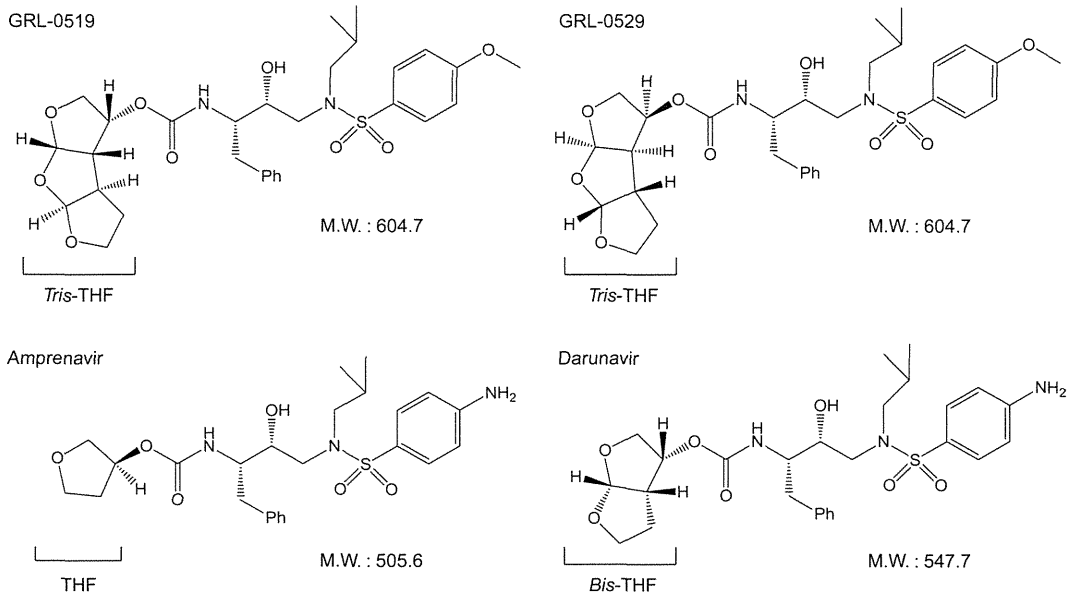

FIG 1 Structures of GRL-0519, GRL-0529, amprenavir, and darunavir. M.W., molecular weight.

strains and primary clinical isolates, including multi-PI-resistant variants with minimal cytotoxicity. In addition, GRL-0519 was active against HIV-2_{ROD}, as well as HIV-1 isolates examined. We also selected HIV-1 variants with GRL-0519 by propagating a laboratory wild-type HIV-1_{NL4-3} in MT-4 cells in the presence of increasing concentrations of GRL-0519 and determined the amino acid substitutions that emerged under the pressure of GRL-0519 in the protease-encoding region. In addition, we evaluated the effects of nonspecific binding of physiological human serum proteins on GRL-0519's anti-HIV-1 activity. We further analyzed the previously published crystal structure of GRL-0519 with protease (Protein Data Bank [PDB] ID, 3OK9) to gain a better understanding of the present antiviral data. The crystal structure analyses indicated that GRL-0519 has strong polar interactions with key residues in the active site of the protease. GRL-0519 also has several water-mediated polar interactions and tight van der Waals interactions with protease residues, suggesting that GRL-0519 binds very tightly in the active site of the protease.

MATERIALS AND METHODS

Cells and viruses. MT-2 and MT-4 cells were grown in RPMI 1640-based culture medium supplemented with 10% fetal calf serum (FCS) (JRH Biosciences, Lenexa, MD), 50 units/ml penicillin, and 100 μg/ml kanamycin. The following HIV strains were employed for the drug susceptibility assay (see below): HIV-1_{LAI}, HIV-1_{NL4-3}, HIV-2_{ROD}, HIV-$1_{ERS104pre}$ (18), clinical HIV-1 strains isolated from drug-naive patients with AIDS, and six HIV-1 clinical strains that were originally isolated from patients with AIDS who had received 9 to 11 anti-HIV-1 drugs over the past 32 to 83 months and that were genotypically and phenotypically characterized as multi-PI-resistant HIV-1 variants (19, 20). All primary HIV-1 strains were passaged once or twice in 3-day-old phytohemagglutinin-activated peripheral blood mononuclear cells (PHA-PBM), and the virus-containing culture supernatants were stored at −80°C until they were used as sources of infectious virions.

Antiviral agents and human serum proteins. Roche Products Ltd. (Welwyn Garden City, United Kingdom) and Abbott Laboratories (Abbott Park, IL) kindly provided saquinavir (SQV) and ritonavir (RTV), respectively. Amprenavir (APV) was a courtesy gift from GlaxoSmithKline, Research Triangle Park, NC. Lopinavir (LPV) was kindly provided by Japan Energy Inc., Tokyo, Japan. Atazanavir (ATV) was a contribution from Bristol Myers Squibb (New York, NY). Darunavir (DRV) was synthesized as previously described (21). Human serum albumin (HSA) and α1-acid glycoprotein (AAG) were purchased from Sigma-Aldrich (St. Louis, MO).

Drug susceptibility assay. The susceptibility of HIV-1_{LAI} or HIV-2_{ROD} to various drugs was determined as previously described with minor modifications. Briefly, MT-2 cells (10^4/ml) were exposed to 100 50% tissue culture infectious doses ($TCID_{50}$) of HIV-1_{LAI} or HIV-2_{ROD} in the presence or absence of various concentrations of drugs in 96-well microculture plates and incubated at 37°C for 7 days. After incubation, 100 μl of the medium was removed from each well and 3-(4,5-dimetylthiazol-2-yl)-2,5-diphenyltetrazolium bromide (MTT) solution (10 μl, 7.5 mg/ml in phosphate-buffered saline) was added to each well in the plate, followed by incubation at 37°C for 2 h. After incubation to dissolve the formazan crystals, 100 μl of acidified isopropanol containing 4% (vol/vol) Triton X-100 was added to each well, and the optical density was measured in a kinetic microplate reader (Vmax; Molecular Devices, Sunnyvale, CA). All assays were performed in duplicate or triplicate. In some experiments, MT-2 cells were chosen as target cells in the MTT assay, since these cells undergo greater HIV-1-elicited cytopathic effects than MT-4 cells. To determine the sensitivity of primary HIV-1 isolates to drugs, PHA-PBM (10^6/ml) were exposed to 50 $TCID_{50}$ of each primary HIV-1 isolate and cultured in the presence or absence of various concentrations of drugs in 10-fold serial dilutions in 96-well microculture plates. In determining the drug susceptibilities of certain laboratory HIV-1 strains, MT-4 cells were employed as target cells as previously described, with minor modifications. In brief, MT-4 cells (10^5/ml) were exposed to 100 $TCID_{50}$ of drug-resistant HIV-1 strains in the presence or absence of various concentrations of drugs and incubated at 37°C. On day 7 of culture, the supernatants were harvested and the amounts of p24 (capsid [CA]) Gag protein were determined by using a fully automated chemiluminescent enzyme immunoassay system (Lumipulse F; Fujirebio Inc., Tokyo, Japan) (22, 23). Drug concentrations that suppressed the production of p24 Gag protein by 50% (50% effective concentration [EC_{50}]) were determined by comparison with the p24 production level in a drug-free control cell culture. All assays were performed in duplicate or triplicate. PHA-PBM were derived from a single donor in each independent experiment. Thus, to obtain the data,

three different healthy donors were recruited. For determining the antiretroviral activity and cytotoxicity of a drug, we used the same cells and cultured them for the same 7 days. The MTT assay was employed for HIV-1_{LAI} and HIV-2_{ROD}, while the p24 assay was employed for clinical HIV-1 isolates and drug-resistant HIV-1 strains.

Creation of PI-resistant HIV-1 variants *in vitro*. MT-4 cells (10^5/ml) were exposed to HIV-1_{NL4-3} (500 $TCID_{50}$) and cultured in the presence of various PIs at an initial concentration equal to its EC_{50}. Viral replication was monitored by the determination of the amount of p24 Gag produced by MT-4 cells. The culture supernatants were harvested on day 7 and were used to infect fresh MT-4 cells for the next round of culture in the presence of increasing concentrations of each drug. When the virus began to propagate in the presence of the drug, the drug concentration was increased generally 2- to 3-fold. Proviral DNA samples obtained from the lysates of infected cells were subjected to nucleotide sequencing. This drug selection procedure was carried out until the drug concentration reached 5 μM, as previously described (24–26). In the experiments for selecting drug-resistant variants, MT-4 cells were also exploited as target cells, since HIV-1 in general replicates at higher levels in MT-4 cells than in MT-2 cells, as described above.

Determination of nucleotide sequences. Molecular cloning and determination of the nucleotide sequences of HIV-1 strains passaged in the presence of anti-HIV-1 agents were performed as previously described (24). In brief, high-molecular-weight DNA was extracted from HIV-1-infected MT-4 cells by using the InstaGene Matrix (Bio-Rad Laboratories, Hercules, CA) and was subjected to molecular cloning, followed by sequence determination. The primers used for the first round of PCR with the entire Gag- and protease-encoding regions of the HIV-1 genome were LTR F1 (5′-GAT GCT ACA TAT AAG CAG CTG C-3′) and PR12 (5′-CTC GTG ACA AAT TTC TAC TAA TGC-3′). The first-round PCR mixture consisted of 1 μl of proviral DNA solution, 10 μl of Premix *Taq* (Ex *Taq* version; TaKaRa Bio Inc., Otsu, Japan), and 10 pmol of each of the first PCR primers in a total volume of 20 μl. The PCR conditions used were an initial 3 min at 95°C, followed by 35 cycles of 40 s at 95°C, 20 s at 55°C, and 2 min at 72°C, with a final 10 min of extension at 72°C. The first-round PCR products (1 μl) were used directly in the second round of PCR with primers LTR F2 (5′-GAG ACT CTG GTA ACT AGA GAT C-3′) and KSMA2.1 (5′-CCA TCC CGG GCT TTA ATT TTA CTG GTA C-3′) under the following PCR conditions: an initial 3 min at 95°C, followed by 35 cycles of 30 s at 95°C, 20 s at 55°C, and 2 min at 72°C, with a final 10 min of extension at 72°C (a stick diagram of HIV-1 genome PCR amplification for sequence analysis is shown in Fig. S1 in the supplemental material). The second-round PCR products were purified with spin columns (MicroSpin S-400 HR columns; Amersham Biosciences Corp., Piscataway, NJ), cloned directly, and subjected to sequencing with a model 3130 automated DNA sequencer (Applied Biosystems, Foster City, CA).

Determination of replication kinetics of GRL-0519-resistant HIV-1_{NL4-3} variants and wild-type HIV-1_{NL4-3}. The GRL-0519-resistant variant at passage 37 was propagated in fresh MT-4 cells without GRL-0519 for 7 days, and aliquoted HIV-$1_{519}{}^{R}{}_{P37}$ viral stocks were stored at −80°C until use. MT-4 cells (3.2×10^5) were exposed to the HIV-$1_{519}{}^{R}{}_{P37}$ or wild-type HIV-1_{NL4-3} preparation containing 10 ng/ml p24 in 6-well culture plates for 3 h, and the newly infected MT-4 cells were washed with fresh medium and divided into 4 fractions, each cultured with or without GRL-0519 (final concentration of MT-4 cells, 10^4/ml; drug concentrations, 0, 0.005, 0.01, and 0.015 μM). The amounts of p24 were measured every 2 days for up to 7 days.

Generation of recombinant HIV-1 clones. To generate HIV-1 clones carrying the desired amino acid substitutions, site-directed mutagenesis was performed with a QuikChange site-directed mutagenesis kit (Stratagene, La Jolla, CA), and the amino acid substitution-containing genomic fragments were introduced into pHIV-$1_{NL4-3Sma}$. Determination of the nucleotide sequences of the plasmids confirmed that each clone had the desired amino acid substitution but no unintended amino acid substitutions. Each recombinant plasmid was transfected into COS7 cells with Lipofectamine LTX transfection reagent (Invitrogen, Carlsbad, CA), and the infectious virions thus made were harvested for 72 h after transfection and stored at −80°C until use.

TABLE 1 Antiviral activities of GRL-0519 and -0529 against HIV-1_{LAI} or HIV-2_{ROD}

Compound	EC_{50} (μM)[a]		CC_{50} (μM) (±SD)	Selectivity index[b]
	HIV-1_{LAI}	HIV-2_{ROD}		
GRL-0519	0.0007 ± 0.0005	0.0004 ± 0.0002	44.6 ± 3.5	63,714
GRL-0529	0.33 ± 0.04	0.40 ± 0.06	38.7 ± 3.7	118
SQV	0.026 ± 0.006	0.003 ± 0.001	19.8 ± 2.9	773
APV	0.033 ± 0.002	0.37 ± 0.11	84.7 ± 5.4	2,590
ATV	0.0048 ± 0.0001	0.0077 ± 0.0006	27.6 ± 2.7	5,520
DRV	0.0042 ± 0.0006	0.0088 ± 0.0004	152.7 ± 10.1	36,357

[a] MT-2 cells (10^4/ml) were exposed to 100 $TCID_{50}$ of HIV-1_{LAI} or HIV-2_{ROD} and cultured in the presence of various concentrations of each PI, and the EC_{50} values were determined using the MTT assay. All assays were conducted in duplicate, and the data shown represent mean value (±1 standard deviation [SD]) derived from the results of three independent experiments.

[b] Each selectivity index denotes a ratio of CC_{50} to EC_{50} against HIV-1_{LAI}.

Structural analysis of interactions of GRL-0519 and DRV with protease. The crystal structures of HIV-1 protease complexed with GRL-0519 or DRV were obtained from the protein data bank (PDB ID, 3OK9 and 2IEN, respectively). The inhibitor conformation with the higher occupancy in the crystal structure was considered for analysis. Bond orders were properly assigned to the inhibitor molecules. Hydrogens were added to all the heavy atoms, and their positions were optimized in an OPLS2005 force field (27) with constraints on heavy atom positions. A cutoff distance of 3.0 Å between a polar hydrogen and oxygen or nitrogen was used to determine the presence of hydrogen bonds. The structures were analyzed using Maestro version 9.3 (Schrödinger, LLC, New York, NY, 2012).

RESULTS

Antiviral activities of GRL-0519 and -0529 against HIV-1_{LAI} and HIV-2_{ROD} and their cytotoxicities. We first examined the antiviral potencies of GRL-0519 and -0529 against a variety of HIV-1 isolates. GRL-0529 showed only moderate anti-HIV-1 activity against a laboratory wild-type HIV-1 strain, HIV-1_{LAI}, and an HIV-2 strain, HIV-2_{ROD}, with EC_{50}s of 0.33 and 0.40 μM, respectively (Table 1). Conversely, GRL-0519 was extremely potent against HIV-1_{LAI}, with an EC_{50} of 0.0007 μM compared to other clinically available Food and Drug Administration (FDA)-approved PIs examined, including DRV (Table 1), as assessed with the MTT assay using MT-2 target cells, while its cytotoxicity was evident only at high concentrations (50% cytotoxic concentration [CC_{50}], 44.6 μM) and the selectivity index proved to be highly favorable at 63,714 (Table 1). GRL-0519 was also very potent against HIV-2_{ROD}, with an EC_{50} of 0.0004 μM (Table 1).

GRL-0519 is potent against various PI-selected laboratory HIV-1 variants. We also examined GRL-0519 against an array of HIV-1_{NL4-3} variants, which had been selected by propagating HIV-1_{NL4-3} in the presence of increasing concentrations (up to 5 μM) of each of 4 FDA-approved PIs (RTV, APV, ATV, and LPV) in MT-4 cells (24). Such variants had acquired various PI resistance-associated amino acid substitutions in the protease-encoding region of the viral genome (Table 2, note *a*). Each variant was highly resistant to the PI by which the variant was selected and showed significant resistance, with an EC_{50} of >1 μM. GRL-0519 was highly active against all the variants (except HIV-$1_{APV}{}^{R}{}_{5\mu M}$), with EC_{50}s of 2.8 to 3.3 nM (differences were 6- to 7-fold greater compared to those against HIV-1_{NL4-3}) (Table 2).

TABLE 2 Antiviral activities of GRL-0519 and -0529 against laboratory PI-resistant HIV-1 variants

Virus[a]	EC_{50} (nM)[b]						
	GRL-0519	GRL-0529	APV	ATV	LPV	TPV	DRV
HIV-1_{NL4-3}	0.5 ± 0.1	356.3 ± 33.8	24.9 ± 0.1	4.2 ± 1.1	37.8 ± 4.5	362.9 ± 104.4	3.9 ± 0.6
HIV-$1_{RTV^R 5\mu M}$	2.8 ± 0.4 (6)	504.3 ± 26.6 (1)	532.9 ± 25.9 (21)	36.4 ± 3.0 (9)	501.2 ± 44.9 (13)	402.1 ± 56.1 (1)	29.1 ± 2.1 (7)
HIV-$1_{APV^R 5\mu M}$	38.0 ± 0.9 (76)	>1,000 (>3)	>1,000 (>40)	371.0 ± 7.8 (88)	>1,000 (>26)	>1,000 (>3)	368.5 ± 32.4 (94)
HIV-$1_{ATV^R 5\mu M}$	3.3 ± 1.6 (7)	376.9 ± 164.8 (1)	390.0 ± 11.1 (16)	>1,000 (>238)	>1,000 (>26)	>1,000 (>3)	28.1 ± 6.4 (7)
HIV-$1_{LPV^R 5\mu M}$	3.2 ± 0.4 (7)	>1,000 (>3)	420.1 ± 61.9 (17)	35.1 ± 4.7 (8)	>1,000 (>26)	>1,000 (>3)	32.9 ± 1.3 (8)

[a] The amino acid substitutions identified in the protease-encoding region compared to the wild-type HIV-1_{NL4-3} include the following: M46I, V82F, and I84V in HIV-$1_{RTV^R 5\mu M}$; L10F, V32I, M46I, I54 M, A71V, and I84V in HIV-$1_{APV^R 5\mu M}$; L23I, E34Q, K43I, M46I, I50L, G51A, L63P, A71V, V82A, and T91A in HIV-$1_{ATV^R 5\mu M}$; and L10F, M46I, I54V, and V82A in HIV-$1_{LPV^R 5\mu M}$.

[b] The EC_{50} values were determined by using MT-4 cells as target cells. MT-4 cells (10^5/ml) were exposed to 100 $TCID_{50}$ of each HIV-1 strain, and the inhibition of p24 Gag protein production by each drug was used as an endpoint. The numbers in parentheses represent the fold changes of EC_{50}s for each isolate compared to the EC_{50}s for HIV-1_{NL4-3}. All assays were conducted in duplicate or triplicate, and the data shown represent mean values (±1 SD) derived from the results of two or three independent experiments.

GRL-0519 exerts potent activity against highly PI-resistant clinical HIV-1 isolates. In our previous work, we isolated highly multi-PI-resistant primary HIV-1 strains, HIV-$1_{MDR/B}$, HIV-$1_{MDR/C}$, HIV-$1_{MDR/G}$, HIV-$1_{MDR/TM}$, HIV-$1_{MDR/MM}$, and HIV-$1_{MDR/JSL}$, from patients with AIDS who had failed then-existing anti-HIV regimens after receiving 9 to 11 anti-HIV-1 drugs over 32 to 83 months (19, 20). These primary strains contained 9 to 14 amino acid substitutions in the protease-encoding region, which have reportedly been associated with HIV-1 resistance against various PIs (Table 3, note *a*). The potency of APV, ATV, and LPV against such clinical multidrug-resistant HIV-1 strains was significantly compromised, as examined in PHA-PBM as target cells using p24 production inhibition as an endpoint (Table 3). However, GRL-0519 exerted quite potent antiviral activity, and its EC_{50}s against those clinical variants were quite low: 0.8 to 3.4 nM (Table 3). The antiviral activity of GRL-0519 proved to be most potent against the six multidrug-resistant clinical HIV-1 variants examined compared to the four FDA-approved PIs (APV, ATV, LPV, and DRV). We also examined the antiviral activity of GRL-0519 against highly DRV-resistant variants (28). These variants were created using the mixture of 8 highly multi-PI-resistant clinical isolates as a starting HIV-1 source and selected with increasing concentrations of DRV. GRL-0519 maintained its activity against highly DRV-resistant MDR mixtures (EC_{50}, 5.6 to 30.0 nM), being more potent than DRV by 7.8- to 8.5-fold (Table 3). Overall, GRL-0519 exerted stronger antiviral activity against various wild-type HIV-1 strains, drug-resistant variants, and HIV-2 strains than DRV by 5- to 22-fold. Furthermore, GRL-0519 was more potent than APV by 118- to 925-fold against HIV-2_{ROD} and drug-resistant variants (Tables 1 to 3).

Effects of human serum proteins on the antiretroviral activity of GRL-0519. The binding of human serum proteins to a

TABLE 3 Antiviral activities of GRL-0519 and -0529 against multidrug-resistant clinical isolates and highly DRV-resistant MDR mixtures in PHA-PBM

Virus[a]	EC_{50} (nM)[b]					
	GRL-0519	GRL-0529	APV	ATV	LPV	DRV
HIV-$1_{WT/ERS104pre}$	0.6 ± 0.2	347.4 ± 27.3	33.8 ± 5.1	2.7 ± 0.6	31.4 ± 4.2	3.9 ± 0.6
HIV-$1_{MDR/B}$ (X4)	3.4 ± 0.5 (6)	611.8 ± 72.8 (2)	459.4 ± 99.2 (14)	469.7 ± 7.4 (174)	> 1,000 (>32)	27.8 ± 5.9 (7)
HIV-$1_{MDR/C}$ (X4)	0.8 ± 0.2 (1)	514.4 ± 130.6 (1)	346.1 ± 55.2 (10)	38.8 ± 2.8 (14)	436.5 ± 3.5 (14)	10.3 ± 2.4 (3)
HIV-$1_{MDR/G}$ (X4)	2.6 ± 1.3 (4)	655.8 ± 292.9 (2)	462.6 ± 64.5 (14)	19.4 ± 7.5 (7)	181.3 ± 23.0 (6)	27.8 ± 5.2 (7)
HIV-$1_{MDR/TM}$ (X4)	2.1 ± 0.3 (4)	530.0 ± 74.7 (2)	476.4 ± 8.1 (14)	74.5 ± 2.6 (28)	422.9 ± 82.0 (13)	30.0 ± 1.0 (8)
HIV-$1_{MDR/MM}$ (R5)	2.5 ± 0.5 (4)	787.4 ± 251.4 (2)	338.9 ± 15.5 (10)	204.8 ± 23.5 (76)	622.5 ± 82.0 (20)	13.3 ± 6.2 (3)
HIV-$1_{MDR/JSL}$ (R5)	2.5 ± 0.2 (4)	> 1,000 (>3)	436.3 ± 90.4 (13)	211.3 ± 98.6 (78)	> 1,000 (>32)	22.1 ± 9.3 (6)
HIV-$1_{DRV^R 10P}$	5.6 ± 0.4 (9)	> 1,000 (>3)	> 1,000 (>32)	322.9 ± 10.4 (77)	> 1,000 (>32)	43.4 ± 13.4 (11)
HIV-$1_{DRV^R 20P}$	30.0 ± 9.8 (50)	> 1,000 (>3)	> 1,000 (>32)	> 1,000 (>370)	> 1,000 (>32)	255.2 ± 4.0 (64)

[a] The amino acid substitutions identified in the protease-encoding region compared to the consensus type B sequence cited from the Los Alamos database include the following: L63P in HIV-$1_{ERS104pre}$; L10I, K14R, L33I, M36I, M46I, F53I, K55R, I62V, L63P, A71V, G73S, V82A, L90 M, and I93L in HIV-$1_{MDR/B}$; L10I, I15V, K20R, L24I, M36I, M46L, I54V, I62V, L63P, K70Q,V82A, and L89 M in HIV-$1_{MDR/C}$; L10I, V11I, T12E, I15V, L19I, R41K, M46L, L63P, A71T, V82A, and L90 M in HIV-$1_{MDR/G}$; L10I, K14R, R41K, M46L, I54V, L63P, A71V, V82A, L90 M, and I93L in HIV-$1_{MDR/TM}$; L10I, K43T, M46L, I54V, L63P, A71V, V82A, L90 M, and Q92K in HIV-$1_{MDR/MM}$; L10I, L24I, I33F, E35D, M36I, N37S, M46L, I54V, R57K, I62V, L63P, A71V, G73S, and V82A in HIV-$1_{MDR/JSL}$; L10I, I15V, K20R, L24I, V32I, M36I, M46L, I54V, I62V, L63P, K70Q, V82A, and L88 M in HIV-$1_{DRV^R 10P}$; and L10I, I15V, K20R, L24I, V32I, M36I, M46L, L63P, A71T, V82A, and L88 M in HIV-$1_{DRV^R 20P}$. HIV-$1_{ERS104pre}$ served as a source of wild-type HIV-1. DRV-resistant HIV-1 variants (HIV-$1_{DRV^R 10P}$ and HIV-$1_{DRV^R 20P}$) were selected *in vitro* by propagating a mixture of eight HIV-1_{MDR} isolates in the presence of increasing concentrations of DRV in MT-4 cells. Six of the eight isolates were the same as those described above. Amino acid substitutions identified in proteases of the other two isolates compared to the consensus type B sequence cited from the Los Alamos database include the following: L10I, I15V, E35D, N37E, K45R, I54V, L63P, A71V, V82T, L90 M, I93L, and C95F in HIV-$1_{MDR/A}$; L10R, N37D, M46I, I62V, L63P, A71V, G73S, V74I, V82T, L90 M, and I93L in HIV-$1_{MDR/SS}$.

[b] The EC_{50} values were determined by using PHA-PBM as target cells, and the inhibition of p24 Gag protein production by each drug was used as an endpoint. The numbers in parentheses represent the fold changes of EC_{50}s for each isolate compared to the EC_{50}s for HIV-$1_{ERS104pre}$. All assays were conducted in duplicate or triplicate, and the data shown represent mean values (±1 SD) derived from the results of three independent experiments. PHA-PBM were derived from a single donor in each independent experiment.

TABLE 4 Nonspecific binding effects of human serum proteins on GRL-0519's antiviral activity

Compound	EC_{50} (nM)[a]		
	None	HSA	AAG
GRL-0519	0.6 ± 0.2	1.9 ± 1.1 (3)	2.4 ± 0.3 (4)
GRL-0529	347.4 ± 27.3	351.5 ± 22.7 (2)	649.0 ± 48.9 (2)
APV	31.5 ± 5.5	30.5 ± 2.6 (1)	286.3 ± 14.8 (9)
ATV	2.7 ± 0.6	14.6 ± 1.2 (5)	32.7 ± 15.9 (12)
LPV	31.4 ± 4.2	32.5 ± 2.7 (1)	232.1 ± 15.2 (7)
DRV	3.9 ± 1.0	7.4 ± 1.2 (2)	33.8 ± 3.5 (9)

[a] HSA (40 mg/ml) or AAG (10 μM) was used to evaluate the binding effects of human serum proteins on GRL-519 and -529 antiviral activities. The EC_{50} values against HIV-$1_{ERS104pre}$ with or without HSA or AAG were determined by p24 assay using PHA-PBM as target cells, and the inhibition of p24 Gag production by each drug was used as an endpoint. The numbers in parentheses represent the fold changes of the EC_{50} values compared to the values without HSA or AAG. The data shown represent mean values derived from the results of two or three independent experiments. PBM were derived from a single donor in each independent experiment.

drug is an important determinant of its pharmacological activity *in vivo*, because overly tight binding may result in reducing interactions between the drug and its target (29). We thus determined the effects of the binding of HSA and AAG on GRL-0519's antiretroviral activity *in vitro*. Physiologically normal concentrations of HSA (40 mg/ml) and AAG (10 μM) were used to evaluate their binding effects on GRL-0519's activity against a wild-type clinical isolate, HIV-$1_{ERS104pre}$. All four FDA-approved drugs substantially maintained their activity in the presence of HSA, with reduction of activity by up to 5-fold relative to the activity in the absence of additional HSA (Table 4). The activities of those PIs were reduced in the presence of AAG by 7- to 12-fold (Table 4). However, the binding effects of both HSA and AAG on GRL-0519's activity were insignificant, only a 3- to 4-fold difference. Of note, GRL-0519's EC_{50}s with HSA or AAG (1.9 to 2.4 nM) significantly exceeded those of the four FDA-approved PIs (Table 4).

***In vitro* selection of HIV-1 variants resistant to GRL-0519.** We next attempted to select HIV-1 variants resistant to GRL-0519 by propagating a laboratory HIV-1 strain, HIV-1_{NL4-3}, in MT-4 cells in the presence of increasing concentrations of GRL-0519 as previously described (24). HIV-1_{NL4-3} was initially exposed to 0.0007 μM GRL-0519 and underwent 37 passages, after which the concentration of GRL-0519 was found to have increased 19-fold (0.0131 μM) compared to that at the initiation of selection. Judging from the amounts of p24 Gag protein produced in the culture medium (up to ~282 ng/ml), the replicative capacity of HIV-1_{NL4-3} at passage 37 ($HIV_{519}{}^{R}{}_{P37}$) was thought to have been reasonably well maintained. Compared to the kinetics of the emergence of variants resistant to APV, the emergence of GRL-0519- and DRV-resistant variants was substantially delayed (Fig. 2). Of note, HIV-1 variants resistant to APV and capable of replicating at >5 μM emerged by passage 20, and variants resistant to GRL-0529, replicating at >1 μM, emerged by passage 6, while it became fairly difficult to increase the concentrations of DRV and GRL-0519 around and beyond passage 20, since the virus populations ceased to replicate with further increased concentrations.

The protease-encoding region of the proviral DNA isolated from infected MT-4 cells was cloned and sequenced at passages 6, 13, 22, 29, and 37 under GRL-0519 selection. The sequences of the region cloned and the percent frequency of identical sequences at each passage are depicted in Fig. 3. By passage 13, the wild-type protease gene sequence was seen in 7 of 19 clones, although an N37S substitution was noted in 10 of the 19 clones. However, by passage 22 and beyond, N37S disappeared, and the virus had mostly acquired K43I and A71T substitutions. As the passages proceeded, greater numbers of amino acid substitutions emerged. At passage 29, V82I substitution was seen in 16 of 22 clones, and V82I became dominant by passage 37 (25 of 26 clones). An L33V substitution was also observed in 4 of the 26 clones by passage 37. Reportedly, APV-resistant HIV-1 variants contain V32I, I50V, I54L/M, L76V, I84V, and L90M substitutions (30, 31), and such substitutions were also identified in the present study (data not

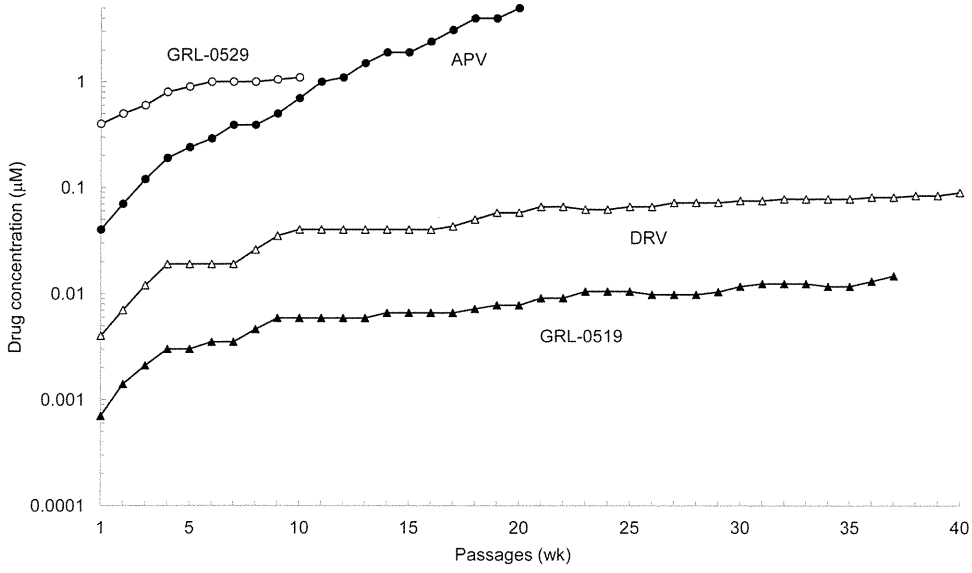

FIG 2 *In vitro* selection of PI-resistant HIV-1 variants. HIV-1_{NL4-3} was propagated in MT-4 cells in the presence of increasing concentrations of amprenavir (●), darunavir (△), GRL-0519 (▲), or GRL-0529 (○). Each passage of virus was conducted in a cell-free manner.

	10 20 30 40 50 60 70 80 90 99	
pNL4-3 PR	PQITLWQRPL VTIKIGGQLK EALLDTGADD TVLEEMNLPG RWKPKMIGGI GGFIKVRQYD QILIEICGHK AIGTVLVGPT PVNIIGRNLL TQIGCTLNF	
6P-1	....	12/16
6P-2	....S.	1/16
6P-3	....S..	1/16
6P-4	....R..	1/16
6P-5	....V... ....A.....	1/16
13P-1	....S...	8/19
13P-2	....	7/19
13P-3	....P.....	1/19
13P-4	....P..... ....S...	1/19
13P-5	....S... ....L.....	1/19
13P-6	....G.....	1/19
22P-1	....I..... .... T.....	10/14
22P-2	....I..... ..... .M..... T.....	1/14
22P-3	....S. ....I..... .... T.....	1/14
22P-4	....V..... .... T.....	1/14
22P-5	....I..... .... T..... ....A...	1/14
29P-1	....I..... .... T..... .I.....	11/22
29P-2	....I..... .... T.....	3/22
29P-3	....T.... ..I..... .... T..... .L.....	1/22
29P-4	....I..... .... T..... .I..... ...C.....	1/22
29P-5	....I..... .... T..... ....A...	1/22
29P-6	....I.... ..I..... .... T..... .I.....	1/22
29P-7	....I..... .... T..... .I..... ..T.....	1/22
29P-8	....M..... ....I.... ..I..... .... T..... .I.....	1/22
29P-9	....G. .....I.... ..I..... .... T..... .I.....S	1/22
29P-10	....I..... .... T..... .T.....	1/22
37P-1	....I..... .... T..... .I.....	17/26
37P-2	....V..... ..I..... .... T..... .I.....	3/26
37P-3	....I...V... .... T..... .I.....	1/26
37P-4	....I..... .... T..... .I..... ..N.....	1/26
37P-5	....V..... .....C. ..... T..... .L.....	1/26
37P-6	....I..... .... T..... .I..... A.....	1/26
37P-7	....A.... ....I..... .... T..... .I..... A...Y....	1/26
37P-8	....V..... ..I..... .... T..... .I.....	1/26

FIG 3 Amino acid sequences of the protease-encoding regions of HIV-1_{NL4-3} variants selected in the presence of GRL-0519. The amino acid sequences of protease, deduced from the nucleotide sequence of the protease-encoding region of each proviral DNA isolated at each indicated time, are shown. The amino acid sequence of the wild-type HIV-1_{NL4-3} protease is illustrated at the top as a reference.

shown). However, no such APV resistance-associated amino acid substitutions emerged during the GRL-0519 selection (Fig. 3). Additionally, HIV-1 selected with GRL-0519 ($HIV_{519}{}^{R}{}_{P37}$) acquired the following Gag amino acid substitutions: E17K and V84A in the matrix (MA) region and G61E and D152N in the CA region.

$HIV_{519}{}^{R}{}_{P37}$ fails to replicate at a low concentration of GRL-0519. Since the replicative capacity of $HIV_{519}{}^{R}{}_{P37}$ was thought to be reasonably well maintained despite the presence of GRL-0519, as mentioned above, we determined the replication kinetics of $HIV_{519}{}^{R}{}_{P37}$ and HIV-1_{NL4-3}. As shown in Fig. 4A, HIV-1_{NL4-3} failed to replicate in the presence of as little as 0.005 μM GRL-0519 during the entire culture period of 7 days. However, $HIV_{519}{}^{R}{}_{P37}$ was capable of replicating in the presence of 0.005 and 0.01 μM GRL-0519, and the amount of p24 produced in the culture

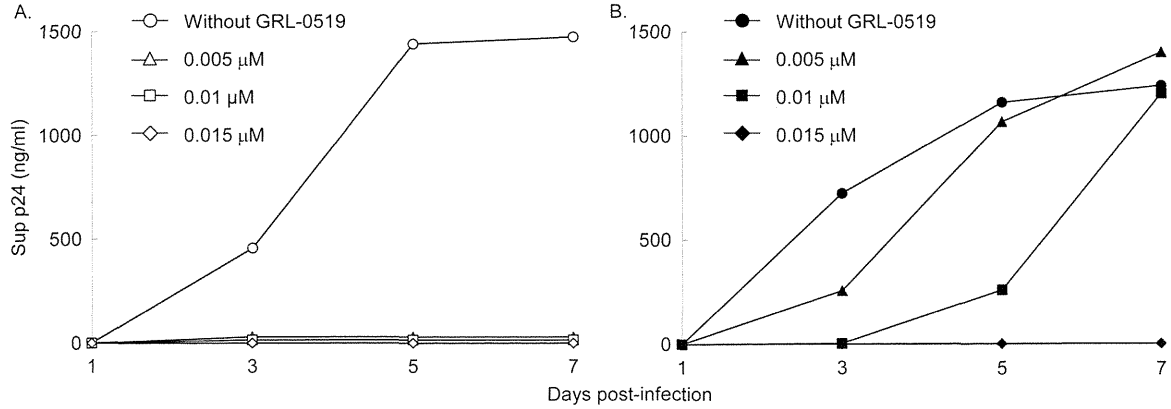

FIG 4 Replication kinetics of HIV-1_{NL4-3} and $HIV_{519}{}^{R}{}_{P37}$. MT-4 cells (3.2×10^5) were exposed to a HIV-1_{NL4-3} or HIV-$1_{519}{}^{R}{}_{P37}$ preparation containing 10 ng/ml p24 in 6-well culture plates for 3 h, and the MT-4 cells were washed with fresh medium and divided into 4 fractions, each cultured with or without GRL-0519 (final concentration of MT-4 cells, 10^4/ml; drug concentrations, 0, 0.005, 0.01, and 0.015 μM). The amount of p24 in each culture flask was measured every 2 days for up to 7 days, once at each time point.

TABLE 5 Roles of 3 amino acid substitutions that emerged during selection with GRL-0519 on GRL-0519's anti-HIV-1 activity

Virus[a]	GRL-0519 EC_{50} (nM)[b]
HIV-1_{NL4-3}	0.5 ± 0.1
HIV-$1_{519}{}^{R}{}_{P37}$	6.0 ± 1.4 (12)
HIV-1_{K43I}	1.2 ± 0.2 (2)
HIV-1_{A71T}	1.4 ± 0.6 (3)
HIV-1_{V82I}	3.2 ± 0.1 (6)

[a] HIV-1_{K43I}, HIV-1_{A71T}, and HIV-1_{V82I} were created using a HIV-1_{NL4-3} plasmid clone.

[b] The EC_{50} values were determined with MT-4 cells, employing a p24 assay. The data shown represent mean values (±1 SD) derived from the results of two or four independent experiments. The numbers in parentheses represent the fold changes of EC_{50}s compared to the value against HIV-1_{NL4-3}.

medium reached the amount without GRL-0519 by day 7. However, $HIV_{519}{}^{R}{}_{P37}$ failed to replicate in the presence of 0.015 μM GRL-0519, and no p24 was detected throughout the culture period (Fig. 4B).

Roles of 3 amino acid substitutions that emerged during selection with GRL-0519 in GRL-0519's anti-HIV-1 activity. We also examined the roles of 3 substitutions that emerged during the GRL-0519 selection experiment, K43I, A71T, and V82I, using single-amino-acid substitutions carrying HIV-1_{NL4-3} variants. First, we determined the exact EC_{50} of GRL-0519 against $HIV_{519}{}^{R}{}_{P37}$ using a p24 assay. GRL-0519 suppressed the replication of $HIV_{519}{}^{R}{}_{P37}$ with an EC_{50} of 6.0 nM, 12-fold different from the EC_{50} against HIV-1_{NL4-3} (Table 5). Next, we determined EC_{50}s of GRL-0519 against 3 single-amino-acid substitution-containing HIV-1_{NL4-3} variants (HIV-1_{K43I}, HIV-1_{A71T}, and HIV-1_{V82I}). GRL-0519 inhibited the replication of HIV-1_{K43I}, HIV-1_{A71T}, and HIV-1_{V82I} with EC_{50}s of 1.2, 1.4, and 3.2 nM, respectively (differences were 2-, 3-, and 6-fold compared to those against HIV-1_{NL4-3}, respectively) (Table 5).

***In vitro* selection of a mixture of 8 HIV-1_{MDR} variants resistant to GRL-0519.** As described above and as shown in Fig. 2, the emergence of HIV-1 variants resistant to GRL-0519 was much delayed, and it took as many as 37 passages (37 weeks) for the virus to acquire its replicative activity in the presence of low concentrations (~0.01 μM). Thus, we attempted to select out GRL-0519-resistant variants using a mixture of 8 multidrug-resistant clinical isolates (HIV-1_{MDR}) as a starting HIV-1 population, as previously described (28, 32). We performed an additional selection experiment with MT4 cells and a mixture of 8 HIV-1_{MDR} variants as a starting virus population, with APV, DRV, and GRL-0519 and -0529. Similar to the results of selection experiments using MT-4 cells and HIV-1_{NL4-3}, the emergence of HIV-1 strains capable of replicating in the presence of GRL-0519 was significantly delayed compared to the cases with APV and DRV (Fig. 5).

Structural analyses of GRL-0519 interactions with protease. We have recently reported the crystal structure depicting the binding mode and interactions of GRL-0519 with protease (17). GRL-0519 has a *tris*-THF moiety as its P2 ligand, and DRV has a *bis*-THF group as its P2 ligand (Fig. 1). Another difference is that GRL-0519 has a methoxybenzene as a P2′ ligand, whereas DRV has an aniline. We analyzed the crystal structure of GRL-0519 with protease and compared it with the structure of protease complexed with DRV. We found that the oxygens of the first and second THF rings of GRL-0519 form hydrogen bond interactions with the backbone amide nitrogens of Asp-29 and Asp-30 in the S2 binding pocket of the protease (Fig. 6A). The urethane NH of GRL-0519 forms a hydrogen bond with Gly-27. The hydroxyl group of GRL-0519 forms hydrogen bonds with the catalytic Asp-25 and Asp-25′. The carbonyl oxygen and the sulfonamide oxygen of GRL-0519 form polar interactions with Ile-50 and Ile-50′ in the protease flap through a bridging water molecule. These interactions are also seen for DRV (Fig. 6B). In fact, the polar interactions with Gly-27, Ile-50, and Ile-50′, as well as with Asp-25 and Asp-25′, are also seen for other protease inhibitors (33, 34). The oxygen of the methoxybenzene (P2′ ligand) of GRL-0519 forms a hydrogen bond with the backbone amide nitrogen of Asp-30′ in the S2′ site of protease. This interaction at the S2′ site is different in the case of DRV. DRV has an aniline as the P2′ ligand, and it forms polar interactions with the backbone carbonyl oxygen of Asp-30′. The third THF ring of the *tris*-THF has water-mediated interactions with Thr-26 and Arg-8 involving 6 bridging water molecules. We also analyzed the van der Waals interactions between GRL-0519 and protease (Fig. 7). The methoxy moiety of GRL-0519 makes good van der Waals contacts with the Asp-29′ and Asp-30′ residues at the S2′ site of protease (Fig. 7A). The contacts seem stronger than the interactions of the corresponding amine group of DRV (Fig. 7B). Analysis of the crystal structure of protease complexed with DRV had suggested that there is room

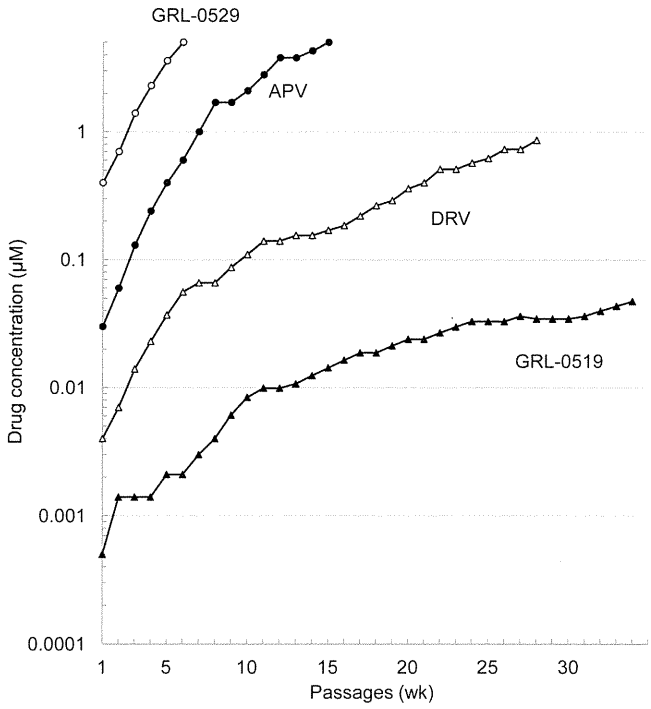

FIG 5 *In vitro* selection using a mixture of 8 multi-PI-resistant HIV-1_{MDR} isolates. A mixture of 8 different multi-PI-resistant clinical HIV-1 isolates was propagated in MT-4 cells in the presence of increasing concentrations of amprenavir (●), darunavir (△), GRL-0519 (▲), or GRL-0529 (○). Each passage of virus was conducted in a cell-free manner. The amino acid substitutions identified in the protease-encoding regions of 2 different multi-PI-resistant clinical isolates compared to the consensus type B sequence cited from the Los Alamos database include L10I, I15V, E35D, N37E, K45R, I54V, L63P, A71V, V82T, L90M, I93L, and C95F in HIV-$1_{MDR/A}$ and L10R, N37D, M46I, I62V, L63P, A71V, G73S, V77IV82T, L90M, and I93L in HIV-$1_{MDR/SS}$. The amino acid substitutions of the other 6 HIV-1_{MDR} variants are given in Table 3, note *a*.

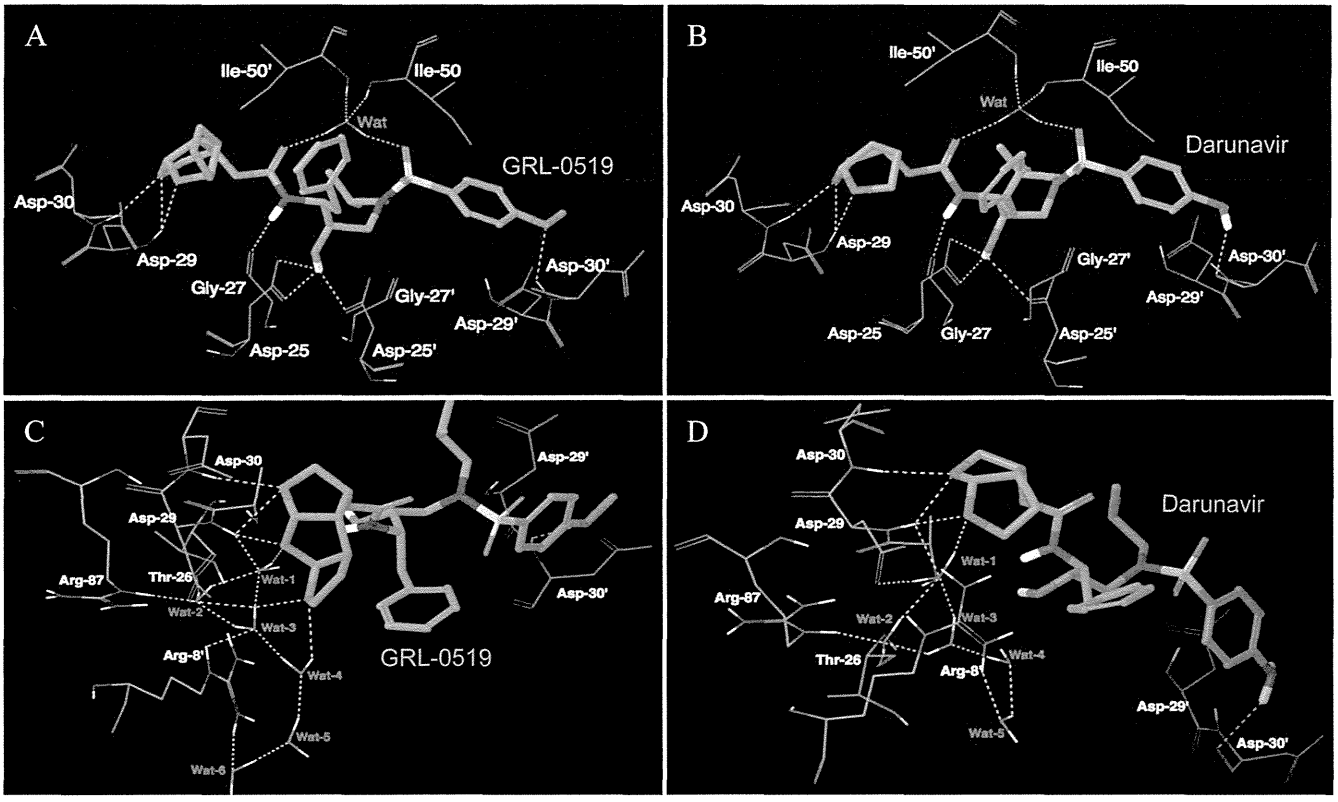

FIG 6 Hydrogen bond interactions of GRL-0519 and darunavir with protease. The interactions between protease–GRL-0519 (PDB ID, 3OK9) and protease-DRV (PDB ID, 2IEN) complexes as determined from their respective crystal structures were analyzed. (A and B) Similar interactions between protease–GRL-0519 (A) and protease-DRV (B) complexes. GRL-0519 has polar interactions with Asp-29, Asp-30, Gly-27, Asp-25, and Asp-25′. It has polar interactions with Ile-50 and Ile-50′ through a bridging water molecule. The protease-DRV complex also has these polar interactions. Both inhibitors have polar interactions with different backbone atoms of Asp-30′ in the S2′ site of the protease. GRL-0519 interacts with the backbone amide nitrogen, whereas DRV interacts with the carbonyl oxygen. (C and D) The interactions of *tris*-THF (C) and *bis*-THF (D) moieties with water molecules highlight differences in the polar interactions of the two inhibitors. The additional THF ring of GRL-0519 interacts with an extra water molecule and has four more polar interactions than DRV. The figures shown here were made with Maestro version 9.3 (Schrödinger, LLC, New York, NY, 2012).

for an extra THF moiety to make additional contacts with protease. The crystal structure examined in the present study confirms that the *tris*-THF fully occupies the binding cavity and forms better van der Waals contacts with protease than the *bis*-THF of DRV (Fig. 7C and D). Contact (C) is defined by the following formula: $C = D_{12}/(R_1 + R_2)$, where D_{12} is the distance between atoms 1 and 2 and R_1 and R_2 are the van der Waals radii of atoms 1 and 2. A good contact is defined as follows: $1.30 > C > 0.89$.

The *tris*-THF moiety increases water-mediated polar interactions with protease. We further analyzed the polar interactions around the *tris*-THF ring of GRL-0519. The crystal structure shows that there are several water molecules that form polar interactions with GRL-0519 and bridge polar interactions with protease (Fig. 6C). Three water molecules, Wat-1, Wat-2, and Wat-3, form a tight network of hydrogen bonds among themselves and mediate polar interactions between GRL-0519 and the active-site residues. Wat-1 directly bridges the polar interactions between the oxygen of the second THF of GRL-0519 and Asp-29. The oxymethyl oxygen of the third THF ring of GRL-0519 enhances the strength of these networks of hydrogen bonds by its polar interactions with Wat-3 and Wat-4 (Fig. 6C). Wat-2 and Wat-3 also bridge the polar interaction between the oxymethyl of the third THF and Arg-87. There is one polar interaction between the third oxymethyl and Arg-8′ through Wat-3 and another network of polar interactions through Wat-4, Wat-5, and Wat-6. The crystal structure of DRV indicates the presence of five water molecules in this region compared to six present for GRL-0519 (Fig. 6D). The *tris*-THF of GRL-0519 and the additional water molecule are responsible for forming a total of 18 hydrogen bonds in this region compared to 14 for DRV, which has a *bis*-THF group as its P2 ligand.

DISCUSSION

GRL-0519, which contains a unique cyclic ether-derived nonpeptide P2 ligand, *tris*-THF, and a sulfonamide isostere, suppressed the replication of a wide spectrum of wild-type HIV-1 and HIV-2 strains with extremely low EC_{50}s (Table 1). GRL-0519 was highly potent against a variety of multidrug-resistant clinical HIV-1 isolates with EC_{50}s ranging from 0.0008 to 0.0034 μM, while the existing FDA-approved PIs examined either failed to suppress the replication of those isolates or required much higher concentrations for viral inhibition (Table 3). GRL-0519 also efficiently blocked, with an EC_{50} of 0.03 μM, the replications of a highly DRV-resistant variant ($HIV_{DRV^{R}P20}$), to which the three PIs (APV, ATV, and LPV) had EC_{50}s of >1 μM and DRV had an EC_{50} of 0.255 μM (Table 3). Moreover, GRL-0519 exerted potent activity

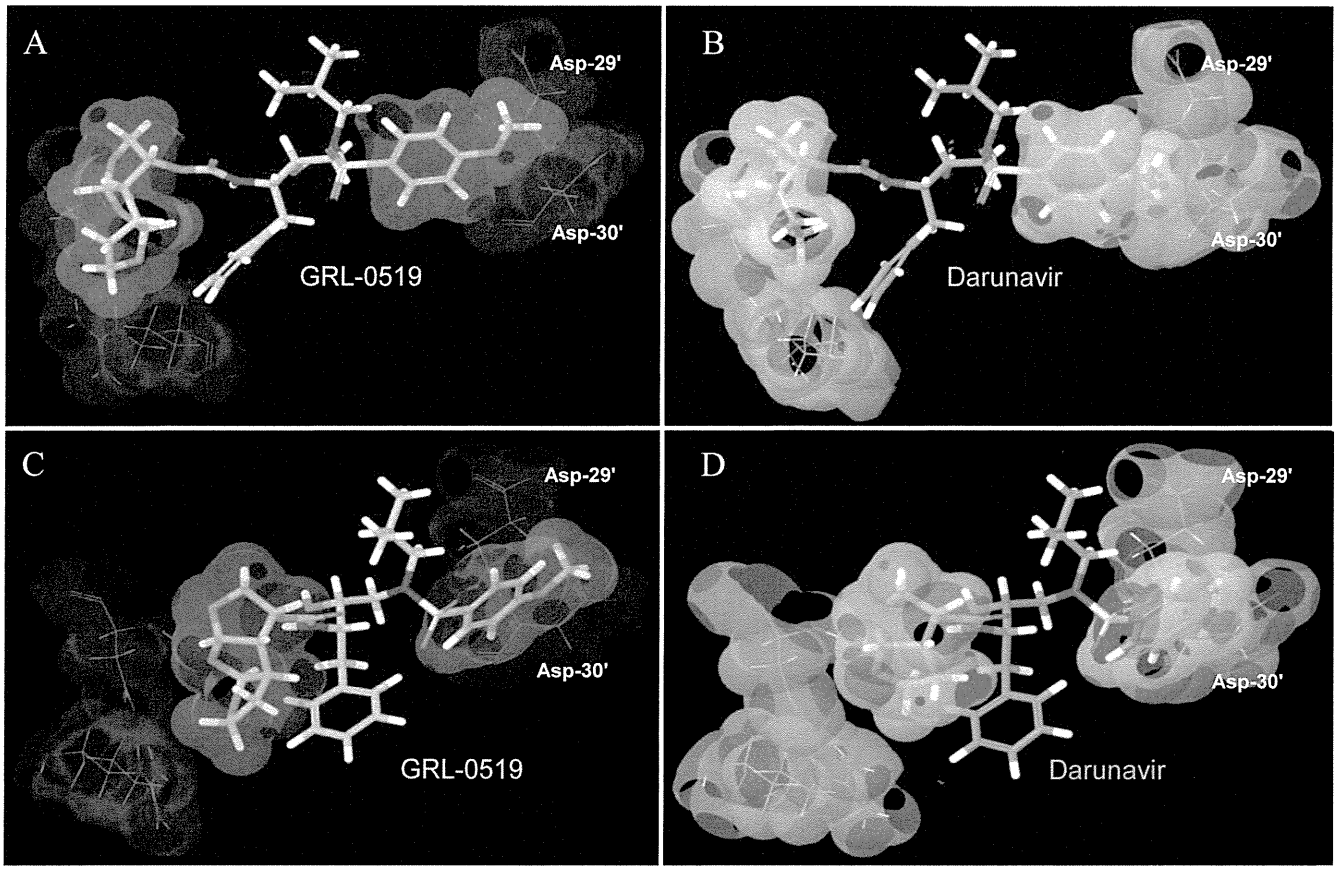

FIG 7 van der Waals interactions of GRL-0519 and darunavir with protease. GRL-0519 is shown as sticks (green carbons), and the van der Waals surfaces of selected moieties of GRL-0519 and its complexed protease are shown in gray and blue, respectively. DRV is shown as sticks (gray carbons), and the van der Waals surfaces of selected moieties of DRV and its complexed protease are shown in yellow and plum, respectively. (A and B) van der Waals interactions between the benzomethoxy of GRL-0519 and Asp-29′ and Asp-30′ of protease (A) and interactions between the aniline of DRV and Asp-29′ and Asp-30′ of protease (B). The surface interactions suggest that the methoxy group of GRL-0519 makes stronger van der Waals interactions with Asp-29′ and Asp-30′ of protease than does DRV. (C and D) The molecules are rotated to show the van der Waals surface interactions of the *tris*-THF (C) and *bis*-THF (D) moieties with protease. The *tris*-THF group of GRL-0519 forms better van der Waals contacts at the S2 site of protease than the *bis*-THF of DRV. The figures were made with Maestro version 9.3 (Schrödinger, LLC, New York, NY, 2012).

against laboratory PI-selected HIV-1 variants (except HIV-$1_{APV}{}^{R}{}_{5\mu M}$) with significantly low EC_{50}s (Table 2). GRL-0519 was less potent against HIV-$1_{APV}{}^{R}{}_{5\ \mu M}$, with an EC_{50} of 38.0 nM (a 76-fold difference), presumably due to the structural resemblance between GRL-0519 and APV, both of which contain a sulfonamide isostere (Fig. 1).

In an attempt to explain why GRL-0519 showed such potent activity against both wild-type and drug-resistant variants, we analyzed the crystal structure of the protease–GRL-0519 complex with protease (PDB ID, 3OK9). GRL-0519 has strong polar interactions with multiple regions of protease (Fig. 6A and C). The oxygens from two of the THF rings of GRL-0519 have strong polar interactions with the backbone amide nitrogens of Asp-29 and Asp-30. GRL-0519 also forms hydrogen bonds with Gly-27 and with the side chains of the catalytic aspartates, Asp-25 and Asp-25′. The sulfonamide oxygen and the carbonyl oxygen form polar contacts with Ile-50 and Ile-50′ in the flap through the bridging water molecule. Comparison of the crystal structures of protease complexes with GRL-0519 and protease complexes with DRV highlights the similarities and differences in interactions between these two inhibitors. The two oxygens from the *bis*-THF of DRV form hydrogen bond interactions with the backbone amide nitrogens of Asp-29 and Asp-30 (Fig. 6B). DRV also forms polar interactions with Gly-27, Asp-25, and Asp-25′ and polar contacts with the protease flap through the bridging water molecule. However, there are important differences in the interactions of GRL-0519 and DRV with protease. An additional water molecule (Wat-3 in Fig. 6C) around the *tris*-THF ring of GRL-0519 is observed in the crystal structure. This water molecule forms hydrogen bond interactions with the third THF ring of GRL-0519 and enhances the polar contact through a network of hydrogen bonds with Asp-29, Thr-26, Arg-87, and Arg-8′. There are four additional polar contacts arising out of the presence of the third THF ring of GRL-0519 and Wat-3 compared to the water-mediated polar interactions in this region of the protease complexes with DRV (Fig. 6D). Even though both GRL-0519 and DRV form polar interactions with the backbone atoms of Asp-30′ in the S2′ site, they interact with different sets of atoms (Fig. 6A and B). GRL-0519 forms the hydrogen bond with the amide nitrogen, whereas DRV forms polar contact with the carbonyl oxygen of Asp30′. The van der Waals surface interactions of GRL-0519 and DRV are also different (Fig. 7A to D). The *tris*-THF and methoxy group of GRL-0519 form

stronger van der Waals contacts with the S2 and S2′ sites of protease, respectively. These interactions are stronger than the corresponding interactions of the *bis*-THF and aniline groups of DRV.

It should be noted that GRL-0519, as previously reported (35), blocks the dimerization of HIV-1 protease monomer subunits more potently, by at least 10-fold, than DRV, as examined by a fluorescence resonance energy transfer (FRET)-based HIV-1 expression assay that uses cyan (CFP) and yellow (YFP) fluorescent protein-tagged protease monomers (17). Considering that the dimerization of HIV-1 protease subunits is an essential process for its acquisition of proteolytic activity, which plays a critical role in the maturation and replication of the virus (36), the potent activity of GRL-0519 to block protease dimerization should also contribute to the greater antiviral potency of GRL-0519 than of DRV. Taken together, the stronger polar and nonpolar contacts of GRL-0519 with protease, as observed in its crystal structure, in addition to its potent activity to block protease dimerization, are likely to be responsible for its much more potent antiviral activity than that of DRV.

In our study, all the PIs examined showed no significant reduction of antiviral activity with the addition of HSA (Table 4). In contrast, the addition of AAG substantially reduced the antiretroviral activities of APV, ATV, and DRV by more than 9-fold, and their EC_{50}s increased to 286.3, 32.7, and 33.8 nM, respectively. However, the reduction with GRL-0519 was only 4-fold, and its absolute EC_{50} was as low as 2.4 nM (Table 4). AAG is an acute-phase protein, and its concentration can increase upon injury, surgery, inflammation, malignancy, and infection, including HIV-1 infection (29, 37). Therefore, this feature of GRL-0519 may represent an advantage for its potential clinical application.

In our HIV-1_{NL4-3} selection experiment using GRL-0519, the emergence of GRL-0519-resistant variants was substantially delayed compared to other PIs and DRV. The use of a mixture of multiple-drug-resistant HIV-1 isolates can expedite the emergence of variants resistant to the drug used for the selection *in vitro* through homologous recombination and should reflect what occurs within individuals harboring a number of drug-resistant HIV-1 species (quasispecies) (28, 32). Thus, in this study, we also employed the mixture of 8 different multi-PI-resistant clinical isolates as a starting viral population (Fig. 5). In the present study, by passage 37, 3 major amino acid substitutions (K43I, A71T, and V82I) were identified in PR of HIV-1_{NL4-3}. The residue V82 is located in the vicinity of the binding pocket of the protease and forms van der Waals contact with GRL0519. The V82A substitution is reportedly associated with resistance against various protease inhibitors (33, 34). However, K43 and A71 are distal from the inhibitor binding pocket and have no direct association with GRL0519. Thus, it is likely K43I and A71T are secondary substitutions. It is particularly noteworthy that we failed to select the A28S amino acid substitution in the present selection experiment with GRL-0519. In our previous studies of potent PIs, such as TMC-126 and GRL-1398, containing a paramethoxy group in the P2′ site, the A28S amino acid substitution was identified as a resistant variant (19, 25). In this regard, the combination of *tris*-THF as the P2 ligand and the paramethoxy moiety at P2′ seems to have prevented the selection of the A28S substitution as a resistant variant.

The *tris*-THF moiety has more interactions with the S2 site of the protease than the *bis*-THF present in either TMC-126 or DRV. Also, the p-OCH3 moiety seems to have more favorable van der Waals interactions with the S2 site than DRV (Fig. 7). It would be reasonable to expect that the combination of *tris*-THF and p-OCH3 may increase the activity, but the antiviral data suggest that GRL-0519 and TMC-126 have essentially the same antiviral activity (see Table S1 in the supplemental material). For any potential antiretroviral agents (including protease inhibitors) to exert their antiretroviral activity even *in vitro*, multiple factors are involved. They include (i) structural stability in culture medium, as well as in the cytoplasm; (ii) permeability into cells; and (iii) compartmentalization. Moreover, such potential antiretroviral agents have to tightly bind to the active site of the target viral protein (i.e., the protease active site) but should not bind to cellular proteins critical to the survival and functionality of the cells. It is possible that while GRL-0519 has greater interactions derived from the presence of the *tris*-THF group, those interactions are not directly reflected in the ultimate antiretroviral activity.

Since the GRL-0519-selected variant, $HIV_{519}{}^{R}{}_{P37}$, was thought to be substantially replication competent, the replication kinetics of HIV-1_{NL4-3} and $HIV_{519}{}^{R}{}_{P37}$ were compared in the presence and absence of GRL-0519. The data showed that HIV-1_{NL4-3} failed to replicate in the presence of 0.005 μM GRL-0519 and that $HIV_{519}{}^{R}{}_{P37}$ did the same in the presence of 0.015 μM GRL-0519 throughout the 7-day culture period (Fig. 4). The concentration range of 0.005 to 0.015 μM is relatively easily achieved in the clinical use of various PIs. For example, the peak and nadir plasma levels of DRV were ~7.1 and 3.4 μM when 400 and 100 mg of DRV/RTV were administered twice daily for 7 days (38). Considering that the EC_{50}s of GRL-0519 are extremely low, ranging from 0.0005 to 0.030 μM (Tables 1 to 4), and that GRL-0519's selectivity index of 63,714 is highly favorable compared to other conventional PIs examined in this study (Table 1), both the anti-HIV potency and safety of GRL-0519 could be favorable, although the efficacy and emergence of adverse effects should be ultimately determined by controlled clinical trials.

In conclusion, GRL-0519 possesses a number of fairly favorable features for the development of the compound as a potential therapeutic for HIV-1 infection and AIDS. However, its oral bioavailability, pharmacokinetics/pharmacodynamics, and biodistribution remain to be determined, and further investigation is warranted.

ACKNOWLEDGMENTS

This work was supported in part by a Grant for Global Education and Research Center Aiming at the Control of AIDS (Global Center of Excellence, supported by Monbu-Kagakusho); Promotion of AIDS Research from the Ministry of Health, Welfare, and Labor of Japan; a Grant to the Cooperative Research Project on Clinical and Epidemiological Studies of Emerging and Reemerging Infectious Diseases (Renkei Jigyo, no. 78; Kumamoto University) of Monbu-Kagakusho (H.M.); the Intramural Research Program of the Center for Cancer Research, National Cancer Institute, National Institutes of Health (H.M.); and by a grant from the National Institutes of Health (GM53386; A.K.G.).

REFERENCES

1. **Edmonds A, Yotebieng M, Lusiama J, Matumona Y, Kitetele F, Napravnik S, Cole SR, Van Rie A, Behets F.** 2011. The effect of highly active antiretroviral therapy on the survival of HIV-infected children in a resource-deprived setting: a cohort study. PLoS Med. 8:e1001044. doi:10.1371/journal.pmed.1001044.
2. **Lohse N, Hansen AB, Gerstoft J, Obel N.** 2007. Improved survival in HIV-infected persons: consequences and perspectives. J. Antimicrob. Chemother. 60:461–463.

3. Mitsuya H, Maeda K, Das D, Ghosh AK. 2008. Development of protease inhibitors and the fight with drug-resistant HIV-1 variants. Adv. Pharmacol. 56:169–197.
4. Walensky RP, Paltiel AD, Losina E, Mercincavage LM, Schackman BR, Sax PE, Weinstein MC, Freedberg KA. 2006. The survival benefits of AIDS treatment in the United States. J. Infect. Dis. 194:11–19.
5. De Clercq E. 2002. Strategies in the design of antiviral drugs. Nat. Rev. Drug Discov. 1:13–25.
6. Siliciano JD, Siliciano RF. 2004. A long-term latent reservoir for HIV-1. J. Antimicrob. Chemother. 54:6–9.
7. Simon V, Ho DD. 2003. HIV-1 dynamics in vivo: implications for therapy. Nat. Rev. Microbiol. 1:181–190.
8. Carr A. 2003. Toxicity of antiretroviral therapy and implications for drug development. Nat. Rev. Drug Discov. 2:624–634.
9. Fumero E, Podzamczer D. 2003. New patterns of HIV-1 resistance during HAART. Clin. Microbiol. Infect. 9:1077–1084.
10. Grabar S, Weiss L, Costagliola D. 2006. HIV infection in older patients in the HAART era. J. Antimicrob. Chemother. 57:4–7.
11. Hirsch HH, Kaufmann G, Sendi P, Battegay M. 2004. Immune reconstitution in HIV-infected patients. Clin. Infect. Dis. 38:1159–1166.
12. Little SJ, Holte S, Routy JP, Daar ES, Markowitz M, Collier AC, Koup RA, Mellors JW, Connick E, Conway B, Kilby M, Wang L, Whitcomb JM, Hellmann NS, Richman DD. 2002. Antiretroviral-drug resistance among patients recently infected with HIV. N. Engl. J. Med. 347:385–394.
13. Naggie S, Hicks C. 2010. Protease inhibitor-based antiretroviral therapy in treatment-naive HIV-1-infected patients: the evidence behind the options. J. Antimicrob. Chemother. 65:1094–1099.
14. Ghosh AK, Kincaid JF, Cho W, Walters DE, Krishnan K, Hussain KA, Koo Y, Cho H, Rudall C, Holland L, Buthod J. 1998. Potent HIV protease inhibitors incorporating high-affinity P2-ligands and (R)-(hydroxyethylamino)sulfonamide isostere. Bioorg. Med. Chem. Lett. 8:687–690.
15. Ghosh AK, Krishnan K, Walters DE, Cho W, Cho H, Koo Y, Trevino J, Holland L, Buthod J. 1998. Structure based design: novel spirocyclic ethers as nonpeptidal P2-ligands for HIV protease inhibitors. Bioorg. Med. Chem. Lett. 8:979–982.
16. Koh Y, Nakata H, Maeda K, Ogata H, Bilcer G, Devasamudram T, Kincaid JF, Boross P, Wang YF, Tie Y, Volarath P, Gaddis L, Harrison RW, Weber IT, Ghosh AK, Mitsuya H. 2003. Novel bis-tetrahydrofuranylurethane-containing nonpeptidic protease inhibitor (PI) UIC-94017 (TMC114) with potent activity against multi-PI-resistant human immunodeficiency virus in vitro. Antimicrob. Agents Chemother. 47:3123–3129.
17. Ghosh AK, Xu CX, Rao KV, Baldridge A, Agniswamy J, Wang YF, Weber IT, Aoki M, Miguel SG, Amano M, Mitsuya H. 2010. Probing multidrug-resistance and protein-ligand interactions with oxatricyclic designed ligands in HIV-1 protease inhibitors. ChemMedChem 5:1850–1854.
18. Shirasaka T, Kavlick MF, Ueno T, Gao WY, Kojima E, Alcaide ML, Chokekijchai S, Roy BM, Arnold E, Yarchoan R, Mitsuya H. 1995. Emergence of human immunodeficiency virus type 1 variants with resistance to multiple dideoxynucleosides in patients receiving therapy with dideoxynucleosides. Proc. Natl. Acad. Sci. U. S. A. 92:2398–2402.
19. Yoshimura K, Kato R, Kavlick MF, Nguyen A, Maroun V, Maeda K, Hussain KA, Ghosh AK, Gulnik SV, Erickson JW, Mitsuya H. 2002. A potent human immunodeficiency virus type 1 protease inhibitor, UIC-94003 (TMC-126), and selection of a novel (A28S) mutation in the protease active site. J. Virol. 76:1349–1358.
20. Yoshimura K, Kato R, Yusa K, Kavlick MF, Maroun V, Nguyen A, Mimoto T, Ueno T, Shintani M, Falloon J, Masur H, Hayashi H, Erickson J, Mitsuya H. 1999. JE-2147: a dipeptide protease inhibitor (PI) that potently inhibits multi-PI-resistant HIV-1. Proc. Natl. Acad. Sci. U. S. A. 96:8675–8680.
21. Ghosh AK, Leshchenko S, Noetzel M. 2004. Stereoselective photochemical 1,3-dioxolane addition to 5-alkoxymethyl-2(5H)-furanone: synthesis of bis-tetrahydrofuranyl ligand for HIV protease inhibitor UIC-94017 (TMC-114). J. Org. Chem. 69:7822–7829.
22. Maeda K, Yoshimura K, Shibayama S, Habashita H, Tada H, Sagawa K, Miyakawa T, Aoki M, Fukushima D, Mitsuya H. 2001. Novel low molecular weight spirodiketopiperazine derivatives potently inhibit R5 HIV-1 infection through their antagonistic effects on CCR5. J. Biol. Chem. 276:35194–35200.
23. Nakata H, Amano M, Koh Y, Kodama E, Yang G, Bailey CM, Kohgo S, Hayakawa H, Matsuoka M, Anderson KS, Cheng YC, Mitsuya H. 2007. Activity against human immunodeficiency virus type 1, intracellular metabolism, and effects on human DNA polymerases of 4′-ethynyl-2-fluoro-2′-deoxyadenosine. Antimicrob. Agents Chemother. 51:2701–2708.
24. Amano M, Koh Y, Das D, Li J, Leschenko S, Wang YF, Boross PI, Weber IT, Ghosh AK, Mitsuya H. 2007. A novel bis-tetrahydrofuranylurethane-containing nonpeptidic protease inhibitor (PI), GRL-98065, is potent against multiple-PI-resistant human immunodeficiency virus in vitro. Antimicrob. Agents Chemother. 51:2143–2155.
25. Ide K, Aoki M, Amano M, Koh Y, Yedidi RS, Das D, Leschenko S, Chapsal B, Ghosh AK, Mitsuya H. 2011. Novel HIV-1 protease inhibitors (PIs) containing a bicyclic P2 functional moiety, tetrahydropyranotetrahydrofuran, that are potent against multi-PI-resistant HIV-1 variants. Antimicrob. Agents Chemother. 55:1717–1727.
26. Tojo Y, Koh Y, Amano M, Aoki M, Das D, Kulkarni S, Anderson DD, Ghosh AK, Mitsuya H. 2010. Novel protease inhibitors (PIs) containing macrocyclic components and 3(R),3a(S),6a(R)-bis-tetrahydrofuranylurethane that are potent against multi-PI-resistant HIV-1 variants in vitro. Antimicrob. Agents Chemother. 54:3460–3470.
27. Kaminski GA, Friesner EA. 2001. Evaluation and reparametrization of the OPLS-AA force field for proteins via comparison with accurate quantum chemical calculations on peptides. J. Phys. Chem. B 105:6474–6487.
28. Koh Y, Amano M, Towata T, Danish M, Leshchenko-Yashchuk S, Das D, Nakayama M, Tojo Y, Ghosh AK, Mitsuya H. 2010. In vitro selection of highly darunavir-resistant and replication-competent HIV-1 variants by using a mixture of clinical HIV-1 isolates resistant to multiple conventional protease inhibitors. J. Virol. 84:11961–11969.
29. Schon A, Ingaramo M, Freire E. 2003. The binding of HIV-1 protease inhibitors to human serum proteins. Biophys. Chem. 105:221–230.
30. Marcelin AG, Affolabi D, Lamotte C, Mohand HA, Delaugerre C, Wirden M, Voujon D, Bossi P, Ktorza N, Bricaire F, Costagliola D, Katlama C, Peytavin G, Calvez V. 2004. Resistance profiles observed in virological failures after 24 weeks of amprenavir/ritonavir containing regimen in protease inhibitor experienced patients. J. Med. Virol. 74:16–20.
31. Young TP, Parkin NT, Stawiski E, Pilot-Matias T, Trinh R, Kempf DJ, Norton M. 2010. Prevalence, mutation patterns, and effects on protease inhibitor susceptibility of the L76V mutation in HIV-1 protease. Antimicrob. Agents Chemother. 54:4903–4906.
32. Aoki M, Danish ML, Aoki-Ogata H, Amano M, Ide K, Koh Y, Mitsuya H. 2012. The loss of protease dimerization inhibition activity of tipranavir (TPV) and its association with HIV-1 acquisition of resistance to TPV. J. Virol. 86:13384–13396.
33. Wlodawer A, Vondrasek J. 1998. Inhibitors of HIV-1 protease: a major success of structure-assisted drug design. Annu. Rev. Biophys. Biomol. Struct. 27:249–284.
34. Wlodawer A, Erickson JW. 1993. Structure-based inhibitors of HIV-1 protease. Annu. Rev. Biochem. 62:543–585.
35. Koh Y, Matsumi S, Das D, Amano M, Davis DA, Li J, Leschenko S, Baldridge A, Shioda T, Yarchoan R, Ghosh AK, Mitsuya H. 2007. Potent inhibition of HIV-1 replication by novel non-peptidyl small molecule inhibitors of protease dimerization. J. Biol. Chem. 282:28709–28720.
36. Dunn BM, Goodenow MM, Gustchina A, Wlodawer A. 2002. Retroviral proteases. Genome Biol. 3:reviews3006.1-reviews3006.7. doi:10.1186/gb-2002-3-4-reviews3006.
37. Fournier T, Medjoubi NN, Porquet D. 2000. Alpha-1-acid glycoprotein. Biochim. Biophys. Acta 1482:157–171.
38. Boffito M, Miralles D, Hill A. 2008. Pharmacokinetics, efficacy, and safety of darunavir/ritonavir 800/100 mg once-daily in treatment-naïve and -experienced patients. HIV Clin. Trials 9:418–427.

1521-0111/12/8201-125–133
MOLECULAR PHARMACOLOGY
U.S. Government work not protected by U.S. copyright
Mol Pharmacol 82:125–133, 2012

Vol. 82, No. 1
78758/3778394

Balancing Antiviral Potency and Host Toxicity: Identifying a Nucleotide Inhibitor with an Optimal Kinetic Phenotype for HIV-1 Reverse Transcriptase

Christal D. Sohl, Rajesh Kasiviswanathan, Jiae Kim, Ugo Pradere, Raymond F. Schinazi, William C. Copeland, Hiroaki Mitsuya, Masanori Baba, and Karen S. Anderson

Department of Pharmacology, School of Medicine, Yale University, New Haven, Connecticut (C.D.S., J.K., K.S.A.); Laboratory of Molecular Genetics, National Institute of Environmental Health Sciences, National Institutes of Health, Research Triangle Park, North Carolina (R.K., W.C.C.); Center for AIDS Research, Department of Pediatrics, School of Medicine, Emory University, and Department of Veterans Affairs, Atlanta, Georgia (U.P., R.F.S.); Departments of Infectious Diseases and Hematology, Kumamoto University Graduate School of Medical Sciences, Kumamoto, Japan (H.M.); Experimental Retrovirology Section, HIV and AIDS Malignancy Branch, National Cancer Institute, National Institutes of Health, Bethesda, Maryland (H.M.); and Division of Antiviral Chemotherapy, Center for Chronic Viral Diseases, Graduate School of Medical and Dental Sciences, Kagoshima University, Kagoshima, Japan (M.B.)

Received March 14, 2012; accepted April 9, 2012

ABSTRACT

Two novel thymidine analogs, 3′-fluoro-3′-deoxythymidine (FLT) and 2′,3′-didehydro-3′-deoxy-4′-ethynylthymidine (Ed4T), have been investigated as nucleoside reverse transcriptase inhibitors (NRTIs) for treatment of HIV infection. Ed4T seems very promising in phase II clinical trials, whereas toxicity halted FLT development during this phase. To understand these different molecular mechanisms of toxicity, pre–steady-state kinetic studies were used to examine the interactions of FLT and Ed4T with wild-type (WT) human mitochondrial DNA polymerase γ (pol γ), which is often associated with NRTI toxicity, as well as the viral target protein, WT HIV-1 reverse transcriptase (RT). We report that Ed4T-triphosphate (TP) is the first analog to be preferred over native nucleotides by RT but to experience negligible incorporation by WT pol γ, with an ideal balance between high antiretroviral efficacy and minimal host toxicity. WT pol γ could discriminate Ed4T-TP from dTTP 12,000-fold better than RT, with only an 8.3-fold difference in discrimination being seen for FLT-TP. A structurally related NRTI, 2′,3′-didehydro-2′,3′-dideoxythymidine, is the only other analog favored by RT over native nucleotides, but it exhibits only a 13-fold difference (compared with 12,000-fold for Ed4T) in discrimination between the two enzymes. We propose that the 4′-ethynyl group of Ed4T serves as an enzyme selectivity moiety, critical for discernment between RT and WT pol γ. We also show that the pol γ mutation R964C, which predisposes patients to mitochondrial toxicity when receiving 2′,3′-didehydro-2′,3′-dideoxythymidine to treat HIV, produced some loss of discrimination for FLT-TP and Ed4T-TP. These molecular mechanisms of analog incorporation, which are critical for understanding pol γ-related toxicity, shed light on the unique toxicity profiles observed during clinical trials.

Introduction

Since the development of AZT in 1985 (Mitsuya et al., 1985), NRTIs have been vital in the treatment of HIV infection. NRTIs inhibit RT by serving as nucleoside mimics; after phosphorylation by cellular kinases, the inhibitors are incorporated into DNA during reverse transcription. Currently available NRTIs lack a 3′-hydroxyl group, and incorporation causes immediate termination of polymerization. Despite the success of NRTIs, limitations include acquired resistance to

This work was supported by the National Institutes of Health Institute of General Medical Sciences [Grants GM049551, GM099289]; the National Institutes of Health Center for Applied Research [Grant 2P30-AI-050409]; the National Institutes of Health National Institute of Environmental Health Sciences Intramural Research program [Grant ES065080]; and the Atlanta Department of Veteran Affairs.

Article, publication date, and citation information can be found at http://molpharm.aspetjournals.org.

http://dx.doi.org/10.1124/mol.112.078758.

ABBREVIATIONS: AZT, zidovudine; NRTI, nucleoside reverse transcriptase inhibitor; FLT, 3′-fluoro-3′-deoxythymidine; Ed4T, 2′,3′-didehydro-3′-deoxy-4′-ethynylthymidine; EFdA, 4′-ethynyl-2-fluoro-2′-deoxyadenosine; WT, wild-type; RT, reverse transcriptase; pol γ, DNA polymerase γ; exo$^+$ pol γ, exonuclease-competent DNA polymerase γ; dT, thymidine; dA, adenine; TP, triphosphate; MP, monophosphate; FDA, U.S. Food and Drug Administration; d4T, 2′,3′-didehydro-2′,3′-dideoxythymidine; k_{exo}, excision rate; k_{pol}, nucleotide incorporation rate; ddA, 2′,3′-dideoxyadenosine; ddC, 2′,3′-dideoxycytidine.

RT and host toxicity, which can manifest as neuropathy, lactic acidosis, and hepatotoxicity (Apostolova et al., 2011).

Although some toxicity can be attributed to mechanisms such as inhibition of phosphorylation (Apostolova et al., 2011), the primary cause of NRTI toxicity is inhibition of human mitochondrial DNA polymerase γ (pol γ) (Kohler and Lewis, 2007; Koczor and Lewis, 2010). Pol γ, which replicates the human mitochondrial genome, is a heterotrimer containing a catalytic monomer, with polymerization and exonuclease domains, and an accessory homodimer, which improves incorporation efficiency and processivity (Johnson et al., 2000; Lee et al., 2009). Pol γ is a member of the A family of DNA polymerases, which are most similar to RT because of fold commonalities and conserved active site residues (Bienstock and Copeland, 2004). Therefore, pol γ is more prone to insert NRTIs during replication, and side effects are often indicators of mitochondrial toxicity (Brinkman et al., 1999).

The dT-analog NRTIs AZT and d4T (stavudine) have been approved by the FDA for treatment of HIV infection but are plagued by toxicity (Lee et al., 2003), which highlights the need for safer NRTIs. Two dT analogs [i.e., FLT and Ed4T (festinavir)] have been under investigation (Fig. 1). In vitro work showed that FLT inhibited viral replication more effectively than did AZT (Kong et al., 1992), with slow evolution of FLT-resistant mutations in RT (Kim et al., 2001). However, FLT-treated rats experienced mitochondrial DNA depletion (Venhoff et al., 2009). Patient toxicity, including two deaths that resulted from hepatic failure, halted clinical trials in phase II (Flexner et al., 1994). Interest in FLT was renewed somewhat with reports that FLT is effective at lower, less toxic doses (De Clercq, 2010). Phase II clinical trials with Ed4T have proven more promising despite the compound's structural similarity to d4T (which lacks the 4′-ethynyl group), a relatively toxic NRTI that inhibits pol γ (Johnson et al., 2001; Bailey et al., 2009). In vitro studies showed that Ed4T is 5 times more potent and significantly less toxic than d4T (Dutschman et al., 2004; Paintsil et al., 2007), and development of RT resistance is slow (Yang et al., 2009).

Despite documented mitochondrial toxicity for FLT, and the potential for mitochondrial toxicity for Ed4T because of structural similarity to d4T, studies directly probing their interactions with pol γ in relation to RT are limited. Often NRTI potency comes at the expense of toxicity resulting from increased WT pol γ inhibition; therefore, both limited analog incorporation by WT pol γ and efficient incorporation by RT are vital. The ideal balance of potency and toxicity involves more efficient analog incorporation compared with native nucleotides by RT and negligible analog incorporation by WT pol γ. However, this has not yet been achieved.

Previous steady-state studies showed that FLT-TP and Ed4T-TP interact with RT and WT pol γ. Unfortunately, steady-state experiments provide information only on the rate-limiting step of catalysis. For these two polymerases, the rate of polymerization is masked by the slow product-release step. Complete characterization of the analog kinetic profiles was needed, including the analog affinity and incorporation rates for both enzymes and the rates of analog removal by pol γ. Pre–steady-state kinetic data were required to generate these molecular mechanisms of toxicity, which correspond well to the degree of mitochondrial toxicity observed among patients (Johnson et al., 2001). We also examined the R964C pol γ mutant, because patients with this mutation, which is located in the polymerase domain of the pol γ catalytic subunit, exhibit higher rates of mitochondrial toxicity when using d4T (Yamanaka et al., 2007).

We found that WT pol γ was 1400-fold better at distinguishing Ed4T-TP from dTTP than distinguishing FLT-TP from dTTP, and this specificity was moderately impaired in R964C pol γ. Conversely, RT preferred Ed4T-TP to FLT-TP and dTTP. It is noteworthy that Ed4T-TP is the first analog to show this exemplary balance of preferred incorporation by RT and negligible incorporation by WT pol γ. We propose that the didehydro ring of Ed4T (and d4T) is important for achieving impaired discrimination in RT, whereas the 4′-ethynyl group serves as an enzyme selectivity moiety that supports the high level of discrimination by WT pol γ. The unique kinetic mechanisms of interaction for FLT and Ed4T help explain the high levels of toxicity observed for FLT and predict lower levels of toxicity for Ed4T.

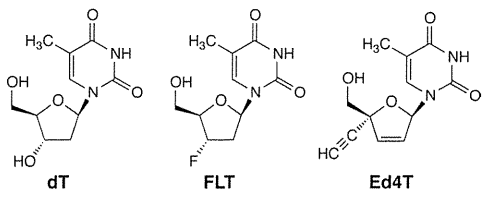

Fig. 1. Structures of dT and its analogs.

Materials and Methods

Reagents. dTTP was purchased from GE Healthcare (Chalfont St. Giles, Buckinghamshire, UK). Triphosphate versions of FLT and Ed4T were prepared as described previously (Ray et al., 2002c). The DNA oligonucleotides D22 (5′-GCCTCGCAGCCGTCCAACCAAC-3′) and D45 (3′-CGGAGCGTCGGCAGGTTGGTTGAGTTGGAGCTAGGTTACGGCAGG-5′) were purchased from Integrated DNA Technologies, Inc. (Coralville, IA) and were purified on 20% polyacrylamide denaturing gels. T4 polynucleotide kinase (New England Biolabs, Ipswich, MA) was used to label the D22 oligonucleotide at the 5′ terminus with [γ-^{32}P]ATP (PerkinElmer Life and Analytical Sciences, Waltham, MA). This D22 primer was then annealed to the D45 template, as described previously (Ray et al., 2002a), to generate the DNA primer/template substrate.

Enzymes. The recombinant WT accessory subunit of pol γ was expressed and purified as described previously (Johnson et al., 2000). All pol γ catalytic subunits used contained an N-terminal hexahistidine tag. The recombinant, exonuclease-deficient, WT catalytic subunit (i.e., WT pol γ) was expressed and purified as described previously (Graziewicz et al., 2004), with minor modifications in the strategy for chromatography. Specifically, WT pol γ was eluted from a nickel column by using a linear gradient of 20 to 400 mM imidazole. The recombinant exonuclease-competent pol γ catalytic subunit (exo$^+$ pol γ) was expressed and purified as described previously (Longley et al., 1998; Lim et al., 2003; Kasiviswanathan et al., 2010). Site-directed mutagenesis was used to generate the R964C pol γ construct, and the recombinant protein was expressed and purified as detailed elsewhere (Kasiviswanathan et al., 2010).

The recombinant RT (p66/p51 heterodimer) clone was kindly provided by Drs. Stephen Hughes and Andrea Ferris (Frederick Cancer Research and Development Center, Frederick, MD). The C-terminal hexa-histidine-tagged RT was purified as described previously (Kerr and Anderson, 1997; Kim et al., 2012). The purity of all proteins, as judged through SDS-polyacrylamide gel electrophoresis with Coomassie staining, was >90%.

Single-Nucleotide Incorporation Assays. Single-nucleotide incorporation experiments were performed by using a KinTek RQF-3

rapid chemical quench apparatus (KinTek Corp., Austin, TX) operated at 37°C. To determine the active-site concentration of each of the enzymes used, dTTP incorporation into the D22/D45 primer/template substrate was examined under burst conditions, as described previously (Murakami et al., 2003). Single-turnover conditions were used to examine the rates of dTTP, FLT-TP, and Ed4T-TP incorporation. For incorporation by WT pol γ and R964C pol γ, 100 nM pol γ catalytic subunit (active-site concentration) was preincubated with an excess of pol γ accessory subunit (4-fold higher concentration than the total, non–active-site, concentration of the catalytic subunit). Holoenzyme (heterotrimer) at 100 nM and 25 nM DNA primer/template substrate in pol γ reaction buffer (50 mM Tris, pH 7.8 at 37°C, 100 mM NaCl) were rapidly mixed with 2.5 mM $MgCl_2$ and varying concentrations of dTTP or analog. Single-nucleotide incorporation experiments with RT were performed in the same manner as the pol γ experiments except that 100 nM RT was used instead of pol γ holoenzyme. Reported concentrations are final (after mixing). After pre–steady-state time periods, the reactions were quenched with 0.3 M EDTA, pH 8.0, and the products were separated on 20% polyacrylamide denaturing gels (0.4 mm thick; 8 M urea). After quantification through filmless autoradiographic analysis with a Bio-Rad Molecular Imager FX (Bio-Rad, Hercules, CA), Kaleidagraph software (Synergy Software, Reading, PA) was used to fit plots of product concentrations versus time to a single exponential equation: product concentration = $A[1 - \exp(-k_{obs}t)]$, where A is the amplitude, k_{obs} is the observed first-order rate constant for dTTP or analog incorporation, and t is the reaction time. The k_{obs} values were plotted against nucleotide concentrations to generate the maximal nucleotide incorporation rate (k_{pol}) and K_d (i.e., the dissociation constant for the nucleotide at the enzyme-primer/template substrate complex) through fitting to a hyperbolic equation: $k_{obs} = (k_{pol} \times \text{dNTP concentration})/(K_d + \text{dNTP concentration})$, with Kaleidagraph software.

Excision Reactions. To incorporate FLT-TP into the 5′-radiolabeled D22/D45 primer/template substrate, 8.0 μM FLT-TP, 5.0 μM DNA primer/template substrate, 1 μM WT pol γ holoenzyme, and 10 mM $MgCl_2$ were incubated for 3 h in pol γ reaction buffer at 37°C. For Ed4T-TP incorporation, 30 μM Ed4T-TP, 5.0 μM DNA primer/template substrate, 1.0 μM RT, and 10 mM $MgCl_2$ were incubated for 2 h in RT reaction buffer (50 mM Tris, pH 7.8 at 37°C, 50 mM NaCl) at 37°C. The reactions were optimized such that the analog incorporation reaction achieved completion. The remaining experimental parameters were the same for both FLT-MP and Ed4T-MP. The incubation mixtures were purified on 20% denaturing polyacrylamide sequencing gels (8 M urea) and, by using filmless autoradiographic analysis, the radiolabeled band, corresponding to D22 with the analog incorporated at position 23 (D22-FLT-MP or D22-Ed4T-MP), was removed. The DNA was extracted from the gel through gentle mixing overnight at room temperature, in a solution containing 0.5 M ammonium acetate, 20 mM magnesium acetate, 1 mM EDTA, and 0.1% SDS. After ethanol extraction (with a 75% ethanol solution for 4 h at −80°C) and drying, the D22-analog primer was rephosphorylated and reannealed as described previously, to generate the DNA primer-analog/template substrate (Ray et al., 2002a). An incubation of 150 nM exo^+ pol γ holoenzyme and 112 nM DNA primer-analog/template substrate in pol γ reaction buffer was manually mixed with 5 mM $MgCl_2$ to initiate the excision reaction at 37°C, under single-turnover conditions. All reported concentrations are final (after mixing). Aliquots of the mixture were removed at various time points and quenched with 0.3 M EDTA, pH 8.0. A 20% denaturing polyacrylamide sequencing gel (0.4 mm thick, 8 M urea) was used to separate the products, and filmless autoradiographic analysis was used to quantify the loss of substrate. A plot of percent substrate versus time was fit to a single exponential decay equation to generate the excision rate (k_{exo}). For Ed4T-MP excision, the plot was fit to a Boltzman sigmoidal equation, and the inflection point concentration was used to determine the half-life, which is proportional to k_{exo} under pseudo-first-order kinetics.

Results

FLT-TP and Ed4T-TP Discrimination by WT pol γ. A critical component of the in vitro toxicity profiles for novel NRTIs is the extent of incorporation by WT pol γ. Previous data on the interactions of these inhibitors with WT pol γ were limited to IC_{50} of 2.7 μM (Cheng et al., 1987) and K_i of 50 nM (Wińska et al., 2010) for FLT-TP and IC_{50} of 100 μM for Ed4T-TP [100-fold higher than that for d4T-TP (Yang et al., 2007)]. Steady-state kinetic data reflect only the rate-limiting step of catalysis, which is product release for many polymerases, including WT pol γ. Therefore, rate constants associated with polymerization cannot be determined from such studies. We used pre–steady-state kinetic analyses to determine the k_{pol} and K_d for FLT-TP and Ed4T-TP incorporation, relative to dTTP.

Under single-turnover conditions, WT pol γ holoenzyme and the DNA primer/template substrate were rapidly mixed with $MgCl_2$ and varying concentrations of dTTP, FLT-TP, or Ed4T-TP for varying times. Triphosphate versions of the drugs were used because the cellular kinases required to phosphorylate the NRTI prodrugs were not present in these in vitro studies. After reaction quenching, the products were separated through gel electrophoresis, and filmless autoradiographic analysis allowed quantification of incorporation of the single correct nucleotide to form the D23 product. The amount of product formed was plotted against the reaction time. This was fit to a single exponential equation to generate the observed rate of nucleotide incorporation, k_{obs}, at each concentration (Fig. 2). These k_{obs} values were then plotted against nucleotide incorporation and fit to a hyperbola to generate k_{pol} and K_d values (Fig. 3).

WT pol γ was able to incorporate dTTP with very high efficiency. The k_{pol} for FLT-TP incorporation by WT pol γ was ~260-fold slower than that for dTTP incorporation (Table 1). However, the affinity for FLT-TP was actually 7.5-fold greater than that for dTTP, which means that WT pol γ preferred the nucleoside analog on the basis of K_d alone. Because of this finding, the overall efficiency of FLT-TP incorporation was only 35-fold lower than that of dTTP incorporation, which indicates that FLT-TP may serve as a substrate for WT pol γ in vivo to a modest but significant extent. This kinetic profile of FLT-TP interaction with WT pol γ supports the evidence of mitochondrial toxicity in vitro (de Baar et al., 2007) and in vivo (Venhoff et al., 2009).

Ed4T-TP demonstrated a different kinetic mechanism of interaction with WT pol γ, compared with that seen for FLT-TP. The k_{pol} for Ed4T-TP incorporation was 2100-fold and 7.9-fold slower than those for dTTP and FLT-TP, respectively (Table 1). Ed4T-TP also showed superiority to FLT-TP in its weak affinity for WT pol γ, with 3- and 23-fold increases in K_d, compared with dTTP and FLT-TP, respectively. Overall, impressive 6200-fold and 180-fold decreases in incorporation efficiency were seen for Ed4T-TP relative to dTTP and FLT-TP, respectively. This high level of discrimination against Ed4T-TP indicates that incorporation of this inhibitor in the physiological nucleotide milieu, where individual dNTP concentrations range from low micromolar to submillimolar levels in mammalian (rat) mitochondria (Song et al., 2005; Wheeler and Mathews, 2011), probably is a rare event. This is supported by the findings of low toxicity in vitro (Haraguchi et al., 2003; Dutschman et al., 2004; Tanaka et al., 2005).

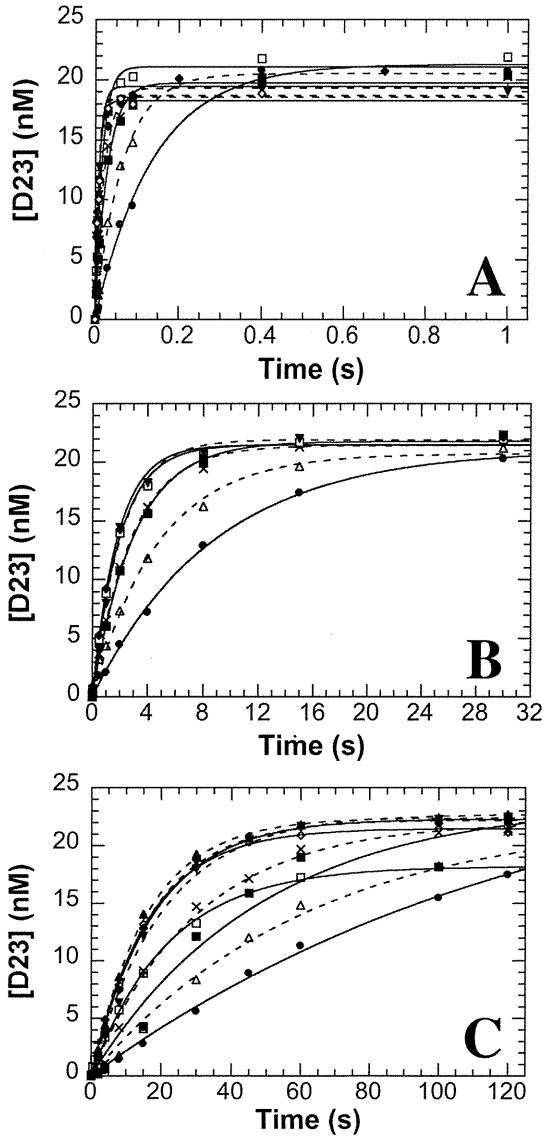

Fig. 2. Observed rates of incorporation by WT pol γ of dTTP or dTTP analogs opposite dA. Each point in the plot represents a single observation, and single exponential equations were used to fit the kinetic traces at varying concentrations of dTTP or dTTP analog. These six to eight experiments all contributed to the k_{pol} and K_d rate constant values. A, incorporation of dTTP. Concentrations of dTTP are denoted as follows: ●, 0.20 μM; △, 0.40 μM; ■, 0.80 μM; ×, 1.5 μM; □, 3.0 μM; ▼, 6.0 μM; ◆, 8 μM; +, 13 μM; ◇, 20 μM. B, incorporation of FLT-TP. Concentrations of FLT-TP are denoted as follows: ●, 0.10 μM; △, 0.25 μM; ■, 0.50 μM; ×, 1.0 μM; □, 2.0 μM; ▼, 5.0 μM; ◆, 8.0 μM. C, incorporation of Ed4T-TP. Concentrations of Ed4T-TP are denoted as follows: ●, 1.5 μM; △, 2.5 μM; ■, 5.0 μM; ×, 8.0 μM; □, 10 μM; ▼, 20 μM; ◆, 30 μM; +, 40 μM; ◇, 50 μM; ▲, 75 μM.

FLT-TP and Ed4T-TP Discrimination by RT. The characterization of the interactions of these analogs with RT is limited, with previous findings including a K_i value of 5 nM for the inhibition of RT by FLT-TP (Cheng et al., 1987) and pre–steady-state studies showing that RT preferred dTTP 1.9-fold over Ed4T-TP, compared with a 4.5-fold preference for dTTP over d4T (Yang et al., 2008). We undertook pre–steady-state, single-turnover experiments in which RT and the DNA-primer/template substrate were rapidly mixed with $MgCl_2$ and varying concentrations of dTTP, FLT-TP, or Ed4T-TP (Fig. 4).

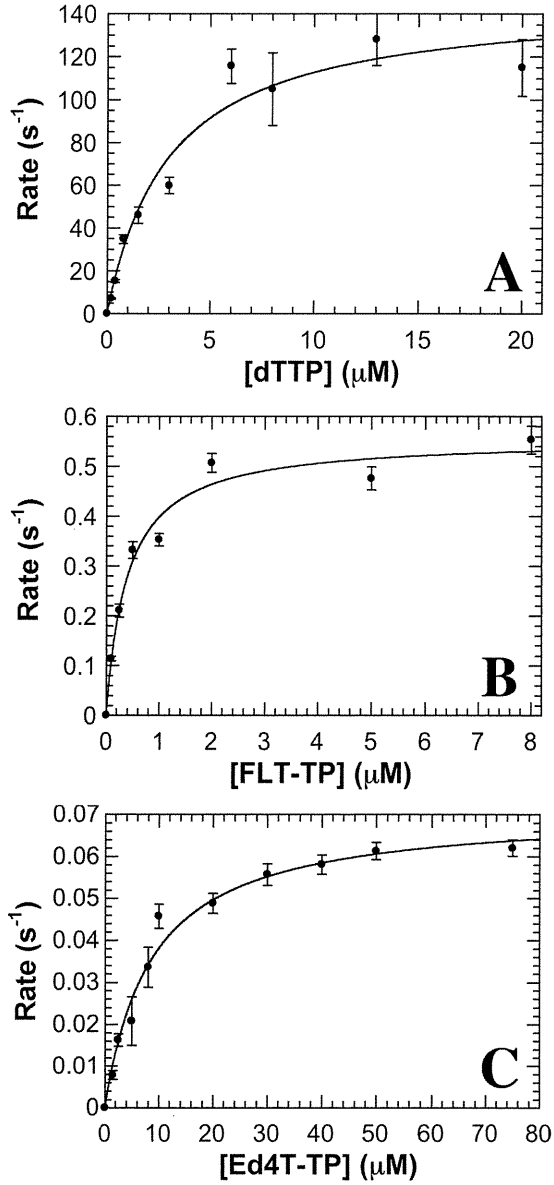

Fig. 3. Nucleotide concentration dependence of the observed rate of WT pol γ incorporation of dTTP analogs opposite dA. Hyperbolic equations were used to fit plots of the observed rate constants (generated from Fig. 2) versus dTTP analog concentrations to obtain k_{pol} and K_d values. Each point represents the observed rate generated from Fig. 2, and the S.E. is the deviance from the hyperbolic fits. Values for k_{pol}, K_d, and efficiency are presented in Table 1. A, incorporation of dTTP. B, incorporation of FLT-TP. C, incorporation of Ed4T-TP.

A 2.2-fold decrease in k_{pol} and a 2-fold increase in K_d were observed for FLT-TP incorporation by RT, relative to dTTP, which resulted in 4.2-fold greater efficiency for dTTP, compared with FLT-TP (Fig. 5 and Table 1). Although there was some preference for the native nucleotide, the incorporation efficiency, which was similar to that for dTTP, indicated that RT would incorporate FLT-TP at significant rates in vivo. The k_{pol} for Ed4T-TP incorporation was identical to that of dTTP. It is noteworthy that the binding affinity was greater, as evidenced by the 2-fold decrease in K_d relative to dTTP, which indicates that RT incorporated Ed4T-TP 2.0-fold more efficiently than dTTP (Fig. 5 and Table 1).

The discrimination by WT pol γ (Table 1) compared favorably with that of RT. RT showed a 8.3-fold loss of discrimi-

TABLE 1
Kinetic parameters for WT pol γ, RT, and R964C pol γ
Efficiency indicates k_{pol}/K_d. Discrimination indicates efficiency$_{dTTP}$/efficiency$_{analog}$.

Enzyme and dTTP Analog	k_{pol}	K_d	Efficiency	Discrimination
	s^{-1}	μM	$\mu M^{-1}\ s^{-1}$	
WT pol γ				
dTTP	147 ± 12	3.0 ± 0.8	49	N.A.
FLT-TP	0.56 ± 0.03	0.40 ± 0.08	1.4	35
Ed4T-TP	0.071 ± 0.003	9 ± 1	0.0079	6200
RT				
dTTP	1.25 ± 0.06	3.0 ± 0.4	0.42	N.A.
FLT-TP	0.58 ± 0.05	6 ± 1	0.1	4.2
Ed4T-TP	1.25 ± 0.05	1.5 ± 0.2	0.83	0.51
R964C pol γ				
dTTP	129 ± 8	3.7 ± 0.7	35	N.A.
FLT-TP	0.51 ± 0.03	0.23 ± 0.06	2.2	16
Ed4T-TP	0.11 ± 0.01	7 ± 2	0.02	1800

N.A., not applicable.

nation for FLT-TP incorporation, relative to WT pol γ, and a striking 12,000-fold decrease in discrimination was seen when Ed4T-TP incorporation by RT was compared with that by WT pol γ. RT is much more likely to incorporate these inhibitors than is WT pol γ. These findings can explain the low toxicity observed to date for Ed4T-TP, although additional clinical testing is needed.

Excision of FLT-MP and Ed4T-MP by exo$^+$ pol γ. An important consideration in the in vitro toxicity profile regarding NRTI incorporation by pol γ is the enzyme's inherent proofreading capability. Nucleoside analog incorporation by pol γ can be essentially negated if excision is efficient. On the basis of nucleoside analog incorporation efficiency, either WT pol γ or RT was used to incorporate a single FLT-TP or a single Ed4T-TP into the DNA primer/template substrate. The D22-FLT-MP/D45 or D22-Ed4T-MP/D45 primer/template was then used as a substrate in the excision reaction. Under single-turnover conditions, exo$^+$ pol γ holoenzyme and the DNA primer-analog/template substrate were manually mixed with $MgCl_2$, and the reaction was quenched after various times. After separation of the products through gel electrophoresis and quantification of the substrate band, the proportion of substrate was plotted versus time (Fig. 6) and the data were fit to a single exponential equation to obtain k_{exo} values, as well as a sigmoidal equation in the case of Ed4T-MP excision (Fig. 6B, inset).

FLT-MP and Ed4T-MP were excised at similar modest rates, although Ed4T-MP excision was slower with the sigmoidal fit (Fig. 6). Half-lives for the exo$^+$ pol γ-D22-analog/D45 complex were 8.8 and 9.6 min for FLT and Ed4T, respectively. These rates of excision were approximately 34-fold slower, on average, than the excision rate for a correctly inserted dT for this primer/template substrate (0.042 s^{-1}) (Feng et al., 2001). However, both analogs were removed more efficiently than ddC and ddA, which have k_{exo} values of 0.0003 s^{-1} (Hanes and Johnson, 2008) and 0.0005 s^{-1} (Johnson et al., 2001), respectively.

FLT-TP and Ed4T-TP Discrimination by R964C pol γ. It was established that d4T-treated patients with the R964C pol γ mutation have higher rates of mitochondrial toxicity (Yamanaka et al., 2007), primarily because of moderate defects in activity and lower levels of nucleoside analog discrimination (Bailey et al., 2009). To determine whether such alterations in pol γ activity were extended to other dTTP analogs, the single-turnover, pre–steady-state experiments performed with WT pol γ were repeated with the R964C pol γ holoenzyme (Fig. 7). Such studies are important to determine whether patients with the R964C pol γ mutation who receive FLT or Ed4T are at higher risk for mitochondrial toxicity.

The incorporation efficiency of dTTP decreased only slightly (1.4-fold) relative to WT pol γ (Table 1), which is consistent with the 1.5-fold loss of efficiency measured previously (Bailey et al., 2009). R964C pol γ was able to incorporate FLT-TP with slightly (1.6-fold) higher efficiency than WT pol γ, and Ed4T-TP was incorporated 2.5-fold more efficiently by R964C pol γ than by WT pol γ (Table 1). When overall discrimination (which takes into account defects in dTTP incorporation) was considered, R964C pol γ showed 2.2-fold and 3.4-fold decreases in discrimination for FLT-TP and Ed4T-TP, respectively, relative to WT pol γ (Table 1).

Discussion

The interactions of FLT-TP and Ed4T-TP with WT pol γ and RT were unique, which clarified the reported differences in toxicity. The incorporation of FLT-TP by WT pol γ was 35-fold slower than that of dTTP, similar to findings for the more toxic NRTIs on the market, compared with the 1000- to nearly 1,000,000-fold slower incorporation for other low-toxicity inhibitors (Table 2). This indicates that some toxicity results from FLT-TP incorporation. On the basis of affinity alone, FLT-TP was preferred over dTTP by WT pol γ. Studies examining the potential for toxicity have focused on pol γ with the analog as a substrate, but we propose that this low K_d indicates that the mitochondrial toxicity observed for FLT may result from direct inhibition. It is likely to be more complex than simple competition, because it was shown that FLT-TP is a noncompetitive inhibitor of pol γ (Wińska et al., 2010). It was proposed that mitochondrial toxicity results in part from competitive inhibition of host thymidine kinase 2 by FLT (Wang et al., 2011), and it is likely that many factors contribute to FLT toxicity.

Ideally, discrimination against dNTP analogs by WT pol γ would be high, whereas discrimination by RT would be low. This would indicate that WT pol γ could readily distinguish among NRTIs and native nucleotides, whereas RT could not. There is only a slight preference for dTTP over FLT-TP with RT, which compares favorably to data for many FDA-approved NRTIs and inhibitors under development (Table 2).